Accelerometer Data Analysis and Presentation Techniques

Melissa J. B. Rogers, Kenneth Hrovat, Kevin McPherson*,
Milton E. Moskowitz, Timothy Reckart

Tal-Cut Company at NASA Lewis Research Center, Cleveland, Ohio 44135
**NASA Lewis Research Center, Cleveland, Ohio 44135*

September 1997

Abstract

The NASA Lewis Research Center's Principal Investigator Microgravity Services project analyzes Orbital Acceleration Research Experiment and Space Acceleration Measurement System data for principal investigators of microgravity experiments. Principal investigators need a thorough understanding of data analysis techniques so that they can request appropriate analyses to best interpret accelerometer data. Accelerometer data sampling and filtering is introduced along with the related topics of resolution and aliasing. Specific information about the Orbital Acceleration Research Experiment and Space Acceleration Measurement System data sampling and filtering is given. Time domain data analysis techniques are discussed and example environment interpretations are made using plots of acceleration versus time, interval average acceleration versus time, interval root-mean-square acceleration versus time, trimmean acceleration versus time, quasi-steady three dimensional histograms, and prediction of quasi-steady levels at different locations. An introduction to Fourier transform theory and windowing is provided along with specific analysis techniques and data interpretations. The frequency domain analyses discussed are power spectral density versus frequency, cumulative root-mean-square acceleration versus frequency, root-mean-square acceleration versus frequency, one-third octave band root-mean-square acceleration versus frequency, and power spectral density versus frequency versus time (spectrogram). Instructions for accessing NASA Lewis Research Center accelerometer data and related information using the internet are provided.

Acronym List

accel	acceleration vector magnitude
a_{CG}	acceleration at the Orbiter center of gravity, mapped from OARE
a_{gg}	acceleration due to gravity gradient effects
a_{ggnew}	acceleration due to gravity gradient effects at a new location
a_{ggOARE}	acceleration due to gravity gradient effects at OARE location
a_{new}	acceleration at a new location, mapped from OARE
a_{OARE}	acceleration at OARE location
a_{rotnew}	acceleration due to rotational effects at a new location
$a_{rotOARE}$	acceleration due to rotational effects at OARE location
avg	subscript denoting average value
CG	center of gravity
cumRMS	subscript denoting cumulative RMS value
dF	frequency resolution (Hertz)
dT	time resolution/sampling interval (seconds)
f	frequency (Hertz)
f_c	filter cutoff frequency (Hertz)
f_{high}	index for upper frequency of frequency band (Hertz)
f_{low}	index for lower frequency of frequency band (Hertz)
f_N	Nyquist frequency (Hertz)
f_s	time series sampling frequency (samples per second)
ftp	file transfer protocol
g	acceleration due to gravity at Earth's surface (9.8 m/s^2)
g_{RMS}	root-mean-square acceleration level
Hz	Hertz
j	$\sqrt{-1}$
k	number of time series intervals used in frequency domain analyses
L	(N-1)/2 if N is odd; (N/2)+1 if N is even
LSLE	Life Sciences Laboratory Equipment
m	subscript for Fourier series; abbreviation for $m\Delta f$
M	number of points in time series interval used in analysis
N	total number of points in a time series

n	subscript for time series index; abbreviation for $n\Delta t$
OARE	Orbital Acceleration Research Experiment
PIMS	Principal Investigator Microgravity Services
PSD	power spectral density
Q	measurement parameter for TMF operations
QTH	quasi-steady three-dimensional histogram
RMS	root-mean-square
RSS	root-sum-of-squares
SAMS	Space Acceleration Measurement System
T	total length of time in time series (seconds)
TMF	trimmean filter
T_p	period of periodic data
U	compensation factor used to account for reduced signal energy resulting from weighting function
w_n	weighting function
(x,y,z)	generic time series axes (may be Orbiter structural coordinate system axes, SAMS triaxial sensor head axes, experiment specific axes)
X_b,Y_b,Z_b	Orbiter body coordinates
X_o,Y_o,Z_o	Orbiter structural coordinates
X_{OARE}, Y_{OARE}, Z_{OARE}	OARE coordinates

Table of Contents

Abstract i
Abbreviations and Acronyms ii
Table of Contents iv
List of Tables v
List of Figures v
1. Introduction 1
2. Data Analysis and Presentation Techniques 1
2.1 Data Sampling, Frequency Limits, Resolution, and Aliasing 2
2.1.1 General Notes 2
2.1.2 OARE and SAMS Sampling and Filtering 3
2.2 Time Domain Analysis 4
2.2.1 Acceleration versus Time 4
2.2.2 Interval Average Acceleration versus Time 5
2.2.3 Interval Root-Mean-Square Acceleration versus Time 6
2.2.4 Trimmean Acceleration versus Time 6
2.2.5 Quasi-steady Three-dimensional Histogram 7
2.2.6 Mapping of OARE Data to Alternate Locations 8
2.3 Fourier Transform Theory and Windowing 8
2.4 Frequency Domain Analysis 10
2.4.1 Power Spectral Density versus Frequency 10
2.4.2 Cumulative RMS Acceleration versus Frequency 11
2.4.3 Root-Mean-Square Acceleration versus Frequency 12
2.4.4 One Third Octave Band RMS Acceleration versus Frequency 12
2.4.5 Power Spectral Density versus Frequency versus Time (Spectrogram) 14
3. Microgravity Measurement and Analysis Information on the Internet 14
3.1 Access to OARE and SAMS Data via File Transfer Protocol 14
3.2 Microgravity Measurement and Analysis WWW Pages 15
4. Summary 15
5. References 16

List of Tables

Table 1. SAMS filter cutoffs and sampling frequencies 3
Table 2. Time domain analysis techniques 4
Table 3. Frequency domain analysis 10
Table 4. Table of 1/3 octave frequency bands 13

List of Figures

Figure 1. Example of aliasing in time domain. Note that both signals have identical values at sampled points, but the frequencies are different. 17
Figure 2. Example of aliasing in frequency domain. Note foldover of spectral components above f_N. For this example, f_S = 50 samples/sec, f_N = 25 Hz. 17
Figure 3. Frequency domain example of aliasing in SAMS data. Upper harmonics of LSLE refrigerator/freezer are folded down to ~2.5 Hz. 18
Figure 4. SAMS acceleration versus time plot. One minute's worth of data. 19
Figure 5. OARE acceleration versus time plot. Twenty hour's worth of data. Note effects of water dump around 2 hours and crew sleep between 11 and 17 hours. 20
Figure 6. SAMS data with 100 second interval average applied. Two hundred minutes of data plotted. Effects of water dump operations are apparent in center of plots. 21
Figure 7. SAMS data with one-second interval average applied. Ten minutes of data plotted. Decrease in levels starting at 450 seconds was caused by cycling off of LSLE refrigerator/freezer compressor. 22
Figure 8. SAMS data with one-second interval RMS applied. Same ten minutes as plotted in Figure 7. Note that the LSLE compressor deactivation is more clearly seen in this plot. 23
Figure 9. OARE data with trimmean filter applied. Same 20 hours as plotted in Figure 5. Note that transients are reduced and the effects of water dumps, attitude maneuvers, and jet activity during crew sleep are more evident in this plot. 24
Figure 10. OARE data collected during LMS mission, displayed as quasi-steady three-dimensional histogram. Two clusters of brighter colors in the left-hand display are indicative of the two Orbiter attitudes maintained during the mission. 25
Figure 11. OARE data with trimmean filter applied. Same 20 hours of data plotted in Figure 5, here mapped to the AGHF (Spacelab) location. 26
Figure 12. Illustration of spectral leakage obscuring the frequency component at 16.68 Hz. 27
Figure 13. Power spectral density calculated using five minutes of SAMS data. No spectral averaging used. 28
Figure 14. Power spectral density calculated using five minutes of SAMS data. The data were divided into nine consecutive segments and the PSDs for the nine segments were averaged together point by point. Compare to Figure 13 which was not averaged. 29

Figure 15. SAMS data displayed as cumulative RMS acceleration versus frequency. Same time period as displayed in Figure 14. Note steps appear in plots at excited frequencies. 30
Figure 16. Individual axes of SAMS data displayed as cumulative RMS acceleration versus frequency. Same period as previous figure. 31
Figure 17. SAMS data displayed as g_{RMS} versus frequency. RMS levels computed for 0.1 Hz wide bands. Same time period as figures 14-16. 32
Figure 18. RSS one third octave RMS acceleration versus frequency using 100 seconds of SAMS data. Bold line is current ISS vibratory requirements curve. 33
Figure 19. Three axes of SAMS data plotted as one third octave RMS acceleration versus frequency. Same time period as Figure 18. 34
Figure 20. Power spectral density versus frequency versus time for two hours of SAMS data. Three axes PSDs were combined using RSS prior to creation of spectrogram. Note cessation of 80 Hz TEMPUS pump 33 minutes into plot and regular cycling of LSLE compressor about 22 Hz (and upper harmonics). 35
Figure 21. SAMS data naming convention. 36
Figure 22. Accessing acceleration data via the Internet from beech.lerc.nasa.gov 37

1. Introduction

The Principal Investigator Microgravity Services (PIMS) project at the NASA Lewis Research Center supports principal investigators of microgravity experiments as they evaluate the effects of varying acceleration levels on their experiments. Upon request, the PIMS team provides acceleration data and data analysis as well as ancillary information pertinent to the microgravity environment measured during experiment operations. PIMS works primarily with data collected by the Orbital Acceleration Research Experiment (OARE) on Columbia and data collected by the Space Acceleration Measurement System (SAMS) on all of the Orbiters and on the Mir space station. Data and information exchange can occur in near real-time during Orbiter missions and before or after Orbiter and Mir missions. Data analysis provided prior to a mission may be used by experimenters and mission planners for experiment timeline planning. Post-mission acceleration data analysis results may be useful in the interpretation of experimental results.

While time series analysis is not a new science, its varied approaches to the interpretation of underlying phenomena may be overwhelming to the experiment investigator who is more interested in analyzing his experimental results than in knowing how to calculate and use a Fourier transform. In this paper, we have attempted to provide an overview of several different data analysis techniques that the PIMS team currently uses for acceleration data. By giving examples of data interpretation using the different analysis techniques, we hope to make it easier for the experimenter to determine what type of analysis to use or to request from the PIMS group. Section 2 describes the different types of data analysis that PIMS currently provides to users. Section 3 provides information about how to obtain PIMS data products and support.

2. Data Analysis and Presentation Techniques

In 1990, Rogers, Alexander, and Snyder prepared a report entitled “Analysis Techniques for Residual Acceleration Data.” In the introduction of that report, they stated:

> There are various aspects of observational data that may be of interest to an investigator, e.g., mean, variance, and minimum and maximum values. Observational data such as . . . accelerometer data are recorded as either continuous time functions or discrete time series. While statistics such as those mentioned above can be obtained from data in this form, additional information can often be obtained by looking at the data from a different perspective, such as can be obtained by transformation of data into a different domain or into different coordinate axes. Of particular interest to us is the analysis of residual acceleration data collected in orbiting space laboratories. A thorough understanding of such data and the ability to manipulate the data will allow the characterization of orbiters so that investigators can better understand the results of low-gravity experiments. [1]

That paper presented many details about Fourier analysis, but did not provide many specifics of how to use frequency domain representations of acceleration data to gain insight into the microgravity environment of orbiting space laboratories. The frequency analysis techniques discussed herein are

mainly extensions of the Fourier analysis and coordinate transformation methods discussed in [1]. Many of the current methods used were derived based on experimenters' requests for a particular piece of information. While there are limits to what information can be obtained from acceleration time series, these basic techniques have given us a rather thorough understanding of the microgravity environment of Earth-orbiting laboratories.

2.1 Data Sampling, Frequency Limits, Resolution, and Aliasing

2.1.1 General Notes

In the analysis of time series, certain restrictions are imposed by the length of the data window being analyzed and by the sampling rate, f_s, used when digitizing continuous data. For a time series segment of length T seconds (N total points), the fundamental period of the segment is assumed to be T, even though the series is not necessarily periodic. This periodicity assumption is intrinsic to the calculation of the Fourier transform, which is the basis for all spectral analysis discussed in this paper. The finest frequency resolution obtainable is $dF=f_s/N$. A lower value of dF is considered better resolution than a higher value of dF. As seen from the expression above, for a given sampling rate, the frequency resolution improves as the number of data points analyzed increases (that is, as a longer segment of data is analyzed). However, there is a trade-off between frequency resolution and spectral variance. Improved frequency resolution comes at the expense of increased spectral variance. The longer the time frame is, the greater the possibility that the spectral content has varied within the segment considered. This is especially true for non-stationary data such as these acceleration measurements recorded on dynamic microgravity platforms. The desire to perform a frequency analysis over a relatively long time period can be achieved by dividing the period into several equal-length blocks and then computing the power spectral density (PSD) of each block. The PSDs for each block can then be laid out in the form of a spectrogram to show intensity versus frequency versus time or they can be averaged to form a single PSD plot, representative of the longer time period. PSDs, spectrograms, and spectral averaging will be discussed later in this document.

Two pieces of information define one segment of time series data: the length of the segment, T, and the sampling interval, dT, used in the acquisition of data. The sampling interval used must be appropriate for the data of interest because it determines the highest frequency component which can be faithfully reconstructed in spectral calculations. This value, f_N, is known as the Nyquist frequency where $f_N = 1/(2dT) = N/(2T)=f_s/2$. Spectral analysis of a time series as described above is confined to the frequency limits $0 \le f \le f_N$. While sampling theory dictates that the data sampling rate be at least two times the highest frequency present in the phenomenon being studied, SAMS typically samples at five times the highest frequency of interest. Attenuation of frequencies below the Nyquist is achieved by means of an anti-aliasing lowpass filter.

From a signal processing point of view, selection of the anti-aliasing lowpass filter's cutoff frequency should be based on the investigator's concern about spectral components less than or equal to the selected cutoff frequency, f_c. This does not mean that structures and materials at the measurement location will not be subjected to the "neglected" portion of the acceleration spectrum above the cutoff frequency. Rather, it was decided a priori that the experiment is not significantly sensitive to these

higher frequency components. Despite lowpass filtering of the data prior to digitization, the acceleration spectrum may contain spectral components above the Nyquist frequency which are strong enough that they are not sufficiently attenuated. This leads to high frequency components being folded-over or aliased to lower frequency artifacts in the frequency regime below f_N. This is illustrated in Figures 1 and 2. While some aliasing is manifest on occasion in SAMS data, it is not commonplace and is typically easy to identify, as seen in Figure 3.

2.1.2 OARE and SAMS Sampling and Filtering

OARE data are sampled at a rate of 10 samples per second following application of a 0.9 Hz lowpass filter to the X_{OARE} axis data and a 0.1 Hz lowpass filter to the Y_{OARE} and Z_{OARE} axis data. The technology of the OARE system allows interpretation of the microgravity environment for the frequency range from 0 Hz up to 1 Hz with a precision of 0.003 micro-g for X_{OARE} and from 0 Hz up to 0.1 Hz with a precision of 0.0046 micro-g for Y_{OARE} and Z_{OARE} .

The triaxial sensor heads on a SAMS unit can be set to record data at several sampling rates ranging from 12.5 to 500 samples per second, see Table 1. The SAMS digitizes the data after applying an anti-aliasing lowpass filter with a 140 dB/decade rolloff. As mentioned earlier, the filter cutoff is typically set to be 1/5 the sampling rate. Other sampling rate / filter cutoff configurations may be set based on experimenter requests. Unidentified offset bias sources lead to uncompensated quasi-steady signals in the SAMS data. These signals can be removed from the SAMS data by a simple de-meaning of the signal prior to the application of any other analysis technique. This de-meaning procedure is not performed during the SAMS data reduction. Therefore, the compensated SAMS data, distributed via internet file server and CD-ROM, still contain this offset bias uncertainty. It is left to the user of the data to remove this artifact. Based on this and the not-fully-quantified noise floor of the SAMS, these data are usually used to interpret the microgravity environment for the frequency range from 0.01 Hz (low end for all sampling rates) up to 100 Hz (high end for f_s=500 samples per second).

Table 1. SAMS filter cutoffs and sampling frequencies

f_c (Hz)	f_s (Hz)
2.5	12.5
5.0	25.0
5.0	50.0
10.0	50.0
25.0	125.0
50.0	250.0
100.0	250.0
100.0	500.0

Because of the inherent differences between OARE and SAMS data, some of the analysis techniques discussed below are more applicable to data from one system than the other. The particular processing technique used depends on the type of information desired. Examples of data interpretation using each analysis technique are provided.

2.2 Time Domain Analysis

The time domain data analysis techniques are acceleration versus time, interval average acceleration versus time, interval root-mean-square (RMS) acceleration versus time, quasi-steady three-dimensional histogram (QTH) of acceleration data, trimmean filtered (TMF) acceleration versus time, and prediction of quasi-steady levels at different locations. All of these options, except the histogram, can be presented on a per axis basis or as a vector magnitude. The quasi-steady histogram and trimmean filtered acceleration calculations are usually prepared using OARE data. Table 2 provides an overview of the time domain analysis techniques discussed here.

Table 2. Time domain analysis techniques

Analysis Technique	***Units***	***Data Typically Used***	***Use***	***Figure #***
Acceleration versus Time	g or fraction of g	OARE SAMS	precise accounting of variation of acceleration magnitude as a function of time	4, 5
Interval Average Acceleration versus Time	g or fraction of g	SAMS	indication of net accelerations lasting for time period ≥ interval parameter	6, 7
Interval RMS Acceleration versus Time	g or fraction of g	SAMS	measure of oscillatory content in data	8
Trimmean Acceleration versus Time	g or fraction of g	OARE	smooth data and reject transient, higher magnitude contributions	9, 11
Quasi-steady Three-dimensional Histogram	percentage of time and g or fraction of g	OARE	summarize acceleration vector magnitude and direction	10
Mapping of OARE Data	g or fraction of g	OARE	predict quasi-steady environment at locations other than OARE sensor	11

2.2.1 Acceleration versus Time

Acceleration magnitude versus time plots show acceleration in units of g versus time. Among the time domain plots discussed in this document, this one yields the most precise accounting of the variation of acceleration magnitude as a function of time. The length of time represented in a plot is usually determined by the focus of the investigation. The sampling rate of the data also influences the plot length. Useful displays can be produced from a couple hours' worth of OARE and lower frequency SAMS data, while SAMS data collected at 25 samples per second or more can best be displayed for periods on the order of seconds or minutes. If a data sampling rate is 125 samples per second, a ten minute plot will have 75000 points. Printing these data with a standard printer at 600 dots per inch requires a 125 inch long paper [2]. This situation is typically avoided, because acceleration versus time plots of SAMS data are usually used to investigate the microgravity environment related to transient or short-lived oscillatory events such as thruster firings or the start-up or shut-down of vibratory equipment.

Figure 4 is an example of SAMS data collected in the Spacelab module during the STS-65 mission. As indicated on the plot, the data were collected with SAMS Triaxial Sensor Head (TSH) C at a rate of 500 samples per second after a 100 Hz lowpass filter was applied to the signal. The data are plotted with respect to the Orbiter structural coordinate system axes. The mean value of each axis is calculated and this value is then subtracted from each data point prior to plotting. The "Original Mean" of the data is indicated to the right of each plot. The data shown in this plot represent the microgravity environment of the Spacelab module during normal experiment operations.

Figure 5 is an example of OARE data collected on the keel bridge of Columbia during the STS-78 mission. The data shown are plotted in Orbiter body coordinates. Note the units of acceleration differ here from the previous SAMS plot in scale. The units here are micro-g. The designator "raw" denotes that this is the acceleration data as recorded at 10 samples per second. During the twenty hours of the mission represented here, four activities of note are captured in this plot. The crew on STS-78 worked on a single shift [3]. The reduction in acceleration levels approximately eleven hours into this plot corresponds to a crew sleep period. Evident throughout the figure, but most prevalent during the sleep period is the signature of the regular vernier reaction control system jet firings to maintain Orbiter attitude. Between hours two and three in the figure, a water dump caused increased acceleration levels, particularly on the Y_b- and Z_b-axes. At the end of the water dump, an attitude maneuver was performed. It is difficult to differentiate this activity from the water dump on this plot.

2.2.2 Interval Average Acceleration versus Time

A plot of the interval average acceleration in units of g versus time gives an indication of net accelerations which last for a number of seconds equal to or greater than the interval parameter. Shorter duration, high amplitude accelerations can also be detected with this type of plot. However, the exact timing and magnitude of specific acceleration events cannot be extracted. The interval average acceleration for the x-axis is defined as

$$x_{avg_k} = \frac{1}{M}\sum_{i=1}^{M} x_{(k-1)M+i} \qquad k = 1, 2, \ldots, \left\lfloor \frac{N}{M} \right\rfloor.$$

Corresponding expressions for the y- and z-axis data can be combined to form the interval average acceleration vector magnitude as follows:

$$\cancel{accel_{avg_k} = \sqrt{x_{avg_k}^2 + y_{avg_k}^2 + z_{avg_k}^2}}$$

Averaging tends to smooth the appearance of the data and allows longer periods of time to be plotted on a single page. This type of display is useful for identifying overall effects of thruster firings and other activities that tend to cause the mean acceleration levels to shift. Although the absolute value of SAMS data is not valid due to the offset bias, relative shifts in the mean levels are valid. Subtle shifts in the dc level are best captured using an interval average plot. Figures 6 and 7 are examples of SAMS data with different interval averaging applied. As shown in Figure 6, a simultaneous waste and supply water dump that is not readily apparent in SAMS acceleration versus time plots, but that was identified through mission timeline information, becomes easily noticeable when we look at the data with a 100 second

interval average. Note the three on/off cycles of the waste water dump that occur during a continuous supply water dump from 60 to 140 minutes on the Y_o-axis plot.

In Figure 7, one second interval averaging was applied to STS-65 data. Note that there is a change in the acceleration signal character approximately 450 seconds into the display, most evident on the Z_o-axis. This change is caused by the duty cycle of the Life Sciences Laboratory Experiment (LSLE) refrigerator/freezer [3,4]. The LSLE has a compressor that operates with a nominal 22 Hz frequency vibration. The compressor motor cycled on and off at regular intervals throughout the mission. The decrease in acceleration levels seen in Figure 7 is due to the cycling off of the compressor.

2.2.3 Interval Root-Mean-Square Acceleration versus Time

A plot of the interval root-mean-square acceleration in units of g versus time gives a measure of the oscillatory content in the acceleration data. For the period of time considered, this quantity gives an indication of the time-averaged power in the signal due to purely oscillatory acceleration sources. The interval RMS acceleration for the x-axis is defined as

$$x_{RMS_k} = \sqrt{\frac{1}{M}\sum_{i=1}^{M}\left(x_{(k-1)M+i)}\right)^2} \qquad k = 1,2,\ldots,\left\lfloor \frac{N}{M} \right\rfloor.$$

Corresponding expressions for the y- and z-axis data can be combined to form the interval RMS acceleration vector magnitude as follows:

$$accel_{RMS_k} = \sqrt{x_{RMS_k}^2 + y_{RMS_k}^2 + z_{RMS_k}^2}\,.$$

Because the interval RMS reduces the amount of data points that represent a period of time, this display allows longer periods of time to be plotted on a single page than acceleration versus time displays. This data representation is useful for identifying changes in background acceleration levels caused by the initiation or cessation of activities such as crew exercise or fan operations.

Figure 8 is an example of SAMS TSH C data from STS-65 with a one second interval RMS operation applied. Note that there is a change in the acceleration signal character approximately 450 seconds into the display, clearly evident on all three axes. This is the same time period shown using interval averaging in Figure 7. The change in the microgravity environment due to the LSLE refrigerator/freezer compressor is more clearly indicated on the interval RMS plot as expected due to its oscillatory nature.

2.2.4 Trimmean Acceleration versus Time

A trimmean filter is applied to raw OARE data to reject transient, higher magnitude accelerations. The objective is to smooth the data to achieve an estimate of the quasi-steady accelerations experienced on Columbia. The TMF utilizes a sliding window to operate on a segment of data of pre-defined length. The sliding window operates such that a segment of the Nth window of data is included in the (N+1)th

window, resulting in some portion of data being considered in two consecutive TMF operations. For most applications, PIMS employs two implementations of the TMF sliding window: 1) 500 sample window of data every 25 seconds and 2) 3000 sample window of data every 8 seconds. Each application of the TMF ranks the collected data in order of increasing magnitude and measures the departure of the distribution from a Gaussian distribution. A parameter, Q, is an estimate of the extent to which the quasi-steady acceleration measurements are contaminated by higher magnitude disturbances (such as thruster firings and crew activity). The Q-parameter is used to choose the amount of data to be trimmed or discarded from the current window of data. The mean of the remaining data is calculated and this value is assigned to the initial time of the window of data being analyzed. Further information can be found in [5].

As with interval average and interval RMS computations, the TMF reduces the number of data points associated with a given period of time, so that longer periods can be displayed on a single plot compared to acceleration versus time displays. This type of analysis is good for highlighting low magnitude, slowly varying components of the microgravity environment such as changes in the aerodynamic drag due to atmospheric density variations.

Figure 9 is an example of OARE data with a trimmean filter applied to 50 seconds of data every 25 seconds. Comparing this plot to Figure 5, it can be seen that the transient disturbances recorded in the raw data, including the regular jet firings, are removed by the TMF operation. The difference between crew sleep and active periods is still obvious, as is the water dump operation. The attitude maneuver three hours into the period is more clear in the TMF data than in the raw data plot.

2.2.5 Quasi-steady Three-dimensional Histogram

The quasi-steady three-dimensional histogram analysis displays a summary of acceleration vector magnitude and alignment projected on three orthogonal planes. These can be top, front, and side views of the Orbiter, or orthogonal planes defined by an experiment configuration [6]. The time series is analyzed using a two-dimensional histogram method where the number of times the acceleration vector magnitude falls within a two-dimensional bin is counted. This is done for each combination of the three orthogonal axes: XY, XZ, and YZ. This count is then divided by the total number of points in the analysis to normalize the result, making comparisons of results amongst several analyses more meaningful. The percentage of time a particular acceleration level occurs is plotted as a color or shade of grey. For the color version, areas showing colors toward the red end of the colorbar indicate a higher number of occurrences of the acceleration vector magnitude falling within that area. Conversely, areas showing colors toward the blue end are indicative of a lower number of occurrences. When comparing QTH plots from separate time periods, care should be taken to check the colorbar for which colors correspond with what percentage of time values. Because these can differ among plots, colors may not be directly comparable.

This type of plot provides a summary of the quasi-steady acceleration vector magnitude and orientation for the total time period analyzed. Exact timing of acceleration events cannot be extracted. It is useful for obtaining an overview of the influence of quasi-steady accelerations during specific scenarios such as a particular Orbiter attitude or water dump operation.

Figure 10 shows a quasi-steady three-dimensional histogram representation of the entire STS-78 mission. The roughly oval, dark blue areas on the three planes of the Orbiter represent the variation of the quasi-steady environment during the mission. The two clusters of color within the ovals are representative of the quasi-steady microgravity environment during the two attitudes in which the Orbiter was maintained during the mission [3, 6].

2.2.6 Mapping of OARE Data to Alternate Locations

Several components of the quasi-steady microgravity environment are easy to predict based on the location being studied, the location of the Orbiter center of gravity (CG), and the Orbiter rotational rates and angles. The atmospheric drag is assumed to be relatively constant for all locations within the Orbiter (this is a rigid-body assumption). Using this assumption, quasi-steady acceleration data collected by OARE can be mapped to other locations in the Orbiter. This mapping is a prediction of what the microgravity environment would be at the alternate location, knowing the acceleration levels at OARE, the distance between OARE and the Orbiter CG (leading to gravity gradient effects, a_{ggOARE}), the distance between the CG and the location of interest (leading to gravity gradient effects, a_{ggnew}), and the Orbiter body rotational rates during the period of interest (leading to rotational effects, a_{rot}) [7, 8].

The data are mapped from the OARE location to the Orbiter CG

$$a_{CG}=a_{OARE}-a_{ggOARE}-a_{rotOARE}$$

and subsequently from the Orbiter CG to the new location

$$a_{new}=a_{CG}+a_{ggnew}+a_{rotnew}$$

This mapping is typically performed in conjunction with the application of a trimmean filter, therefore effects of rotational rate and angle data sampling are smoothed out. Figure 11 shows the data displayed in Figure 9 mapped from the OARE location to the location of the Advanced Gradient Heating Facility in the Spacelab module [3]. Note that the sawblade effect caused by the attitude-maintenance jet firings is more prevalent in the X_b-axis at this location because it is further removed from the Orbiter CG (along the X_b-axis) than the OARE location.

2.3 Fourier Transform Theory and Windowing

Transformation of data to the frequency domain is done to gain more insight about the microgravity environment and to help identify acceleration sources. Analyses that transform data into the frequency domain result in displays of acceleration power spectral density versus frequency, RMS acceleration versus frequency, cumulative RMS acceleration versus frequency, one third octave band RMS acceleration versus frequency, and power spectral density versus frequency versus time (spectrogram). Any of these frequency domain analysis techniques typically performed on SAMS data can be applied to raw OARE data, if desired.

Fourier transformation is a common means of studying time series data in the frequency domain. Following Fourier theory, a function f(t), with fundamental period 2π and satisfying Dirichlet conditions, can be represented by an infinite series of sinusoids, a Fourier series [1, 9-12]. Discrete Fourier transformation is a way to calculate the Fourier coefficients of a given time series. For the time series f_n, n=0, 1, 2, . . ., N-1, the discrete Fourier transform of f_n is

$$F_m = \sum_{n=0}^{N-1} f_n e^{-j2\pi nm/N} \qquad m = 0,1,2,...,(N-1).$$

Fast Fourier Transform methods are designed to efficiently compute the values of F_m shown above.

The fundamental information obtained from Fourier transformation is the relative magnitudes of the various sinusoidal signals that compose the time series. A knowledge of the predominate disturbing frequencies in the microgravity environment is often of interest to experiment investigators. The Fourier transformation is the basis for the power spectral density and other frequency domain analyses discussed in the following section.

When performing frequency domain analyses of data, different types of filters can be applied to achieve different effects. For example, lowpass filters can be applied to accelerometer data to remove higher frequency disturbances that an investigator knows will not affect the experimental results. Bandpass filters can be employed to focus an analysis on a specific, typically narrow, region of the acceleration spectrum. Comb filters enable rejection of a specific frequency and its harmonics. The choice of filter and design of appropriate filter parameters permits the desired manipulation of the data set. No type of filtering after data collection, however, can remove the aliasing effects of improperly sampled data.

In addition to the type of filtering mentioned above, a weighting function can be applied to the time series before spectral analysis is performed to address the problem of spectral leakage. Spectral leakage will arise in the analysis of periodic data with period T_p if the length of the record being analyzed, T, is not an integer number of T_p periods as assumed in Fourier theory. In order to suppress spectral leakage, it is common to introduce a weighting function that tapers the time series data to eliminate discontinuities at the beginning and end of the record. In acceleration data analysis, a Hanning window is typically used to reduce spectral leakage and thus show features more clearly [10-12]. Unless otherwise stated, all the frequency domain analysis displays shown here have had a Hanning window applied. When no windowing is applied to a time series, it is often said that a boxcar window was used. This offers no signal tapering and thus has no effect on spectral leakage.

As demonstrated in Figure 12, when a non-integer number of periods is used to compute the PSD using a boxcar window (the dashed curve), the smearing of a strong spectral component, in this case the Ku-band antenna at about 17 Hz, over the surrounding frequency bins can render close, somewhat weaker components, like the one at 16.68 Hz, virtually undetectable. For comparison, see the solid line in Figure 12 for a PSD of the same dataset using a Hanning window. Notice the spectral peak at 16.68 Hz is now clearly evident.

2.4 Frequency Domain Analysis

Table 3 provides an overview of the frequency domain analysis techniques discussed here.

Table 3. Frequency domain analysis techniques

Analysis Technique	*Units*	*Data Typically Used*	*Use*	*Figure #*
Power Spectral Density versus Frequency	g^2/Hz	SAMS	estimate of distribution of energy with respect to frequency	12, 13, 14
Cumulative RMS Acceleration versus Frequency	g_{RMS}	SAMS	quantifies contributions of spectral components to overall RMS acceleration level for time period studied in cumulative fashion	15, 16
RMS Acceleration versus Frequency	g_{RMS}	SAMS	quantifies contributions of spectral components per frequency bin	17
Spectrogram	g^2/Hz	SAMS	road map of how acceleration signals vary with respect to both time and frequency	3, 20

2.4.1 Power Spectral Density versus Frequency

The power spectral density is computed directly from the Fourier transform of a time series as indicated here [1, 11].

For even N:

$$PSD(m) = \begin{cases} \dfrac{2|F(m)|^2}{N\,U\,f_s} & [\text{units}^2/\text{Hz}] \quad \text{for m} = 1,2,\ldots,(\text{N}/2)-1 \\ \dfrac{|F(m)|^2}{N\,U\,f_s} & [\text{units}^2/\text{Hz}] \quad \text{for m} = 0 \text{ and m} = (\text{N}/2) \end{cases}$$

and for odd N:

$$PSD(m) = \begin{cases} \dfrac{2|F(m)|^2}{N\,U\,f_s} & [\text{units}^2/\text{Hz}] \quad \text{for m} = 1,2,\ldots,(\text{N}-1)/2 \\ \dfrac{|F(m)|^2}{N\,U\,f_s} & [\text{units}^2/\text{Hz}] \quad \text{for m} = 0 \end{cases}$$

where

$$U = \frac{1}{N}\sum_{n=0}^{N-1} w_n^2$$

is the compensation factor [12] used to account for the attenuation of the signal imposed by the weighting function, w_n, applied to suppress spectral leakage. The PSD has units of (units of original function)^2/Hz. For SAMS data, these units are g^2/Hz. This method for computation of the PSD is consistent with Parseval's Theorem, which states that the RMS value of a time signal is equal to the square root of the integral of the PSD across the frequency band represented by the original signal [11]:

$$x_{RMS} = \sqrt{\frac{1}{T}\int_0^T x^2(t)dt} = \sqrt{\int_0^\infty PSD(f)df} \quad .$$

All measured data contain some amount of noise due to characteristics of the measuring, recording, and storage equipment. Such noise tends to mask the underlying signal. Averaging of data is often performed to reduce the influence of such noise on the interpretation of the underlying phenomenon. While the microgravity environment of Earth-orbiting laboratories is not stationary, there are periods when the environment does not change significantly. Spectral averaging (point-by-point averaging of frequency domain spectra) is used to improve the estimation of the spectrum of interest [9].

Welch's Method of spectral averaging is performed by dividing the time period of interest into k equal length intervals. The PSD of each interval is calculated and the k resulting spectral series are averaged together on a point-by-point basis. Spectral averaging following Welch's Method not only reduces the variance of the spectral estimate, but it also tends to smooth the appearance of the spectrum [10]. As can be seen in Figures 13 and 14, spectral averaging results in data plots that are much easier to read and interpret. For accelerometer data frequency domain analyses, some understanding of the aspect of the microgravity environment under investigation (for example, transient thruster firings and continuous, oscillatory fan operations) helps to define the proper window lengths to use, see [9].

Figures 13 and 14 were computed using SAMS TSH C data from STS-65 for the first five minutes of the time period shown in Figures 7 and 8. The total time period (T=5.0 min.) is indicated on the top right corner of Figure 14 and the number of averages this period was divided into is indicated at the top center of the page (k=9). The 22 Hz frequency component present on all three axes is caused by the compressor of the LSLE refrigerator/freezer. Recall that the cessation of LSLE vibrations approximately 450 seconds into Figures 7 and 8 had a marked effect on those two data displays. Other features of note in Figure 14 are the excitation of Orbiter structural modes below 10 Hz, the 17 Hz frequency component caused by the dither of the Orbiter Ku-band communications antenna, upper harmonics of the 17 Hz and 22 Hz disturbances, and several components in the 40 to 100 Hz range with unknown sources [4].

2.4.2 Cumulative RMS Acceleration versus Frequency

A plot of cumulative RMS acceleration in units of g_{RMS} versus frequency quantifies in cumulative fashion the contributions of spectral components to the overall RMS acceleration level for the time frame spanned. Therefore, vertical steps in plots of this type indicate discrete frequencies (or a narrow band of frequencies) that contribute significantly to the acceleration environment, while plateaus are indicative of relatively quiet portions of the spectrum. The x-axis cumulative RMS acceleration is

computed as follows:

$$x_{cumRMS_k} = \sqrt{\sum_{i=1}^{k} PSD_x(i)dF} \qquad k = 1, 2, ..., L.$$

Similar expressions exist for the y- and z-axis data. The overall cumulative RMS acceleration as a function of frequency is computed like so:

$$accel_{cumRMS_k} = \sqrt{x_{cumRMS_k}{}^2 + y_{cumRMS_k}{}^2 + z_{cumRMS_k}{}^2}.$$

Figure 15 shows cumulative RMS acceleration versus frequency plots for the same window of STS-65 SAMS TSH C data shown in Figure 14. Figure 16 shows the computation for the vector magnitude (or root-sum-of-squares, RSS) of the three axes of data. From these displays the microgravity experiment investigator can determine the relative contributions of various disturbances to the overall microgravity environment. The individual axis displays may be particularly important to an investigator whose experiment is sensitive to a particular frequency along a defined direction. In the example of Figure 15, an experiment with an axial sensitivity to 22 Hz vibrations should probably be aligned such that the sensitive axis is parallel to the Orbiter X_o which shows the minimum effect from the LSLE.

2.4.3 Root-Mean-Square Acceleration versus Frequency

By dividing the spectrum into k equal-width frequency bands and computing the g_{RMS} level for each of these bands, we can then plot these values to display the RMS acceleration as a function of frequency. The width of these bands is defined by the user and the results of this type of analysis can be presented in tabular or graphical form.

Figure 17 is an example of a g_{RMS} versus frequency display for the same time period as Figure 15. The RMS levels were computed for consecutive bands of 0.1 Hz width. It is clear that the peaks in Figure 17 are about the same magnitude as the corresponding steps in Figure 15. This would not necessarily be the case if different frequency bandwidths were used in the g_{RMS} calculations.

2.4.4 One Third Octave Band RMS Acceleration versus Frequency

This analysis is a specialized version of the graphical representation of g_{RMS} values computed for specified proportional bandwidth frequency bands. In this case, the (nearly) one third octave bands are those defined by the International Space Station microgravity requirements, see Table 4 [13]. The analysis quantifies the RMS acceleration level contributed by each of the one third octave frequency bands given a 100 second interval. The results of the analysis are typically plotted along with a curve representing the International Space Station combined vibratory limits to compare the acceleration environment to these prescribed limits. The one third octave band RMS acceleration is computed as follows:

$$accel_{RMS_k} = \sqrt{\sum_{i=f_{low(k)}}^{f_{high(k)}} RSS(PSDs(i))dF} \qquad k = 1,2,...,31.$$

Figure 18 shows an RSS one third octave plot of SAMS data collected by TSH C during STS-65. Also shown on the plot are the ISS vibratory requirements limits (the bold stair-step line). The strong RMS level in the one third octave band centered at 25 Hz is primarily due to the LSLE refrigerator/ freezer at about 22 Hz and the excursion in the one third octave band centered at 80.635 Hz is primarily due to the TEMPUS water pump at about 80 Hz. Figure 19 shows the one third octave RMS acceleration versus frequency plots for the X_o, Y_o, and Z_o components of the same data set used to generate Figure 18. Note that when the ISS requirements are interpreted on a per-axis basis, they become less stringent.

Table 4. Table of one third octave frequency bands

f_{low}(Hz)	f_{center}(Hz)	f_{high}(Hz)
0.0891	0.10	0.1122
0.1122	0.125	0.1413
0.1413	0.16	0.1778
0.1778	0.20	0.2239
0.2239	0.25	0.2818
0.2818	0.315	0.3548
0.3548	0.40	0.4467
0.4467	0.50	0.5623
0.5623	0.63	0.7079
0.7079	0.80	0.8913
0.8913	1.00	1.1220
1.1220	1.25	1.4130
1.4130	1.6	1.7780
1.7780	2.00	2.2390
2.2390	2.5	2.8180
2.8180	3.15	3.5480
3.5480	4.0	4.4670
4.4670	5.0	5.6230
5.6230	6.3	7.0790
7.0790	8.0	8.9130
8.9130	10.0	11.220
11.220	12.5	14.130
14.130	16.0	17.780
17.780	20.0	22.390
22.390	25.0	28.180
28.180	31.5	35.480
35.480	40.0	44.670
44.670	50.0	56.230
56.230	64.0	71.838
71.838	80.635	90.510
90.510	101.59	114.04

2.4.5 Power Spectral Density versus Frequency versus Time (Spectrogram)

Spectrograms provide a road map of how acceleration signals vary with respect to both time and frequency. To produce a spectrogram, PSDs are computed for successive intervals of time. The PSDs are oriented vertically on a page such that frequency increases from bottom to top. PSDs from successive time slices are aligned horizontally across the page such that time increases from left to right. Each time-frequency bin is imaged as a color or grey scale corresponding to the logarithm of the PSD magnitude at that time and frequency. Spectrograms are particularly useful in identifying when certain activities begin and end. Figure 20 can be used as an example of how to identify start/termination of an activity (see 22 and 80 Hz regions of spectrogram) and how the frequency components of an activity can vary with time (see 22 Hz region of spectrogram).

3. Microgravity Measurement and Analysis Information on the Internet

3.1 Access to OARE and SAMS Data via File Transfer Protocol

After each mission, SAMS and OARE data are available over the internet from the NASA Lewis Research Center file server beech.lerc.nasa.gov. SAMS data files are typically available 6 to 8 weeks after raw data files are delivered to SAMS. The estimated availability time for SAMS data is 3 months after landing. OARE data files are typically available one month after landing.

Files of SAMS data are organized in a tree-like structure. Data acquired from a mission are categorized based upon sensor head, mission day, and type of data. Data files are stored at the lowest level in the tree and the file name reflects the contents of the file, Figure 21. For example, the file named axm00102.15r contains data for TSH A, the x-axis, the time base was Mission Elapsed Time, day 001, hour 02, 1 of 5 files for that hour, and it contains reduced data. The file readme.doc provides a comprehensive description and guide to the data.

The OARE TMF data are organized into three files, one each for the X_b-, Y_b-, and Z_b-axes. The applicable OARE data are found in the mission directories. Files under the canopus directory are trimmean filter data, computed by Canopus Systems, Inc. Files under the msfc-raw directory contain the telemetry data files provided to PIMS by the Marshall Space Flight Center Payload Operations Control Center data reduction group. Files under the msfc-processed directory are raw files containing binary floating point values, listing the MET (in hours), and the x, y, and z axis acceleration in micro-g's. See the readme files for complete data descriptions.

Also available from the file server are some data access tools for different computer platforms.

The overall structure of the beech file server is given in Figure 22. The file server beech.lerc.nasa.gov can be accessed via anonymous file transfer protocol (ftp), as follows:

a) Establish an ftp connection to the beech file server.
b) Login: anonymous
c) Password: guest
d) Change the directory to pub
e) List the files and directories in the pub directory. There are at least five directories at this level: OARE, SAMS-MIR, SAMS-SHUTTLE, UTILS, and USERS.
f) Change to the directory of choice.
g) Change the directory to the mission of interest, for example: usml-2
h) List the files and directories for the specific mission chosen in the previous step.
i) Use the data file structure to find the files of interest.
j) Enable binary transfer mode.
k) Transfer the data files of interest.

If you encounter difficulty in accessing the data using the file server, please send an electronic mail message to the internet address below. Please describe the nature of the difficulty and a description of the hardware and software you are using to access the file server.

pims@lerc.nasa.gov

Upon request, the PIMS team can provide SAMS data on CD-ROM media. Contact the internet address above for more information.

3.2 Microgravity Measurement and Analysis WWW Pages

The Principal Investigator Microgravity Services, Space Acceleration Measurement System, and Orbital Acceleration Research Experiment projects are all part of the NASA Lewis Research Center's Microgravity Measurements and Analysis Project. More information about these and related projects is available at the URL given below.

http://www.lerc.nasa.gov/WWW/MMAP

4. Summary

Numerous time and frequency domain analysis techniques have been introduced. Examples of SAMS and OARE data interpretation using these techniques are given so that microgravity experimenters are better able to use accelerometer data in experiment planning and in the analysis of their experimental results.

5. References

[1] Rogers, M.J.B., J.I.D. Alexander, R.S. Snyder: Analysis Techniques for Residual Acceleration Data. NASA TM-103507, July 1990.

[2] Liberman, E.M., J.C. Acevedo: Setting Standards in Microacceleration Data Archiving, Dissemination and Microacceleration Information Presentation. Joint Xth European and VIth Russian Symposium on Physical Sciences in Microgravity, St. Petersburg, Russia, 15-21 June 1997.

[3] Hakimzadeh, R., K. Hrovat, K.M. McPherson, M.E. Moskowitz, M.J.B. Rogers: Summary Report of Mission Acceleration Measurements for STS-78. NASA TM-107401, January 1997.

[4] Rogers, M.J.B., R. DeLombard: Summary Report of Mission Acceleration Measurements for STS-65. NASA TM-106871, March 1995.

[5] DeWet, T., J.W.J. VanWyk: Efficiency and Robustness of Hogg's Adaptive Trim Means. Commun. Stastist.-Theor. Meth., A8(2), pp. 117-128, 1979.

[6] DeLombard, R., K. McPherson, M. Moskowitz, K. Hrovat: Comparison Tools for Assessing the Microgravity Environment of Missions, Carriers and Conditions. NASA TM-107446, April 1997.

[7] Blanchard, R.C., J.Y. Nicholson, J.R. Ritter: Absolute Acceleration Measurements on STS-50 from the Orbital Acceleration Research Experiment (OARE). Microgravity Sci. Technol., VII/1, pp. 60-67, 1994.

[8] Blanchard, R.C., J.Y. Nicholson: Orbiter Rarefied-Flow Reentry Measurements from the OARE on STS-62. NASA TM-110182, June 1995.

[9] Karl, J.H.: An Introduction to Digital Signal Processing. Academic Press, Inc., San Diego, 1989.

[10] Oppenheim, A.V., R.W. Schafer: Digital Signal Processing. Prentice-Hall, Inc., Englewood Cliffs, 1975.

[11] Bendat, J.S., A.G. Piersol: Random Data, 2nd edition. John Wiley & Sons, New York, 1986.

[12] Ifeachor, E.C., B.W. Jervis: Digital Signal Processing—A Practical Approach. Addison-Wesley Publishing Company, Wokingham, England, 1993.

[13] NASA System Specification for the International Space Station, Specification Number SSP 41000E, July 1996.

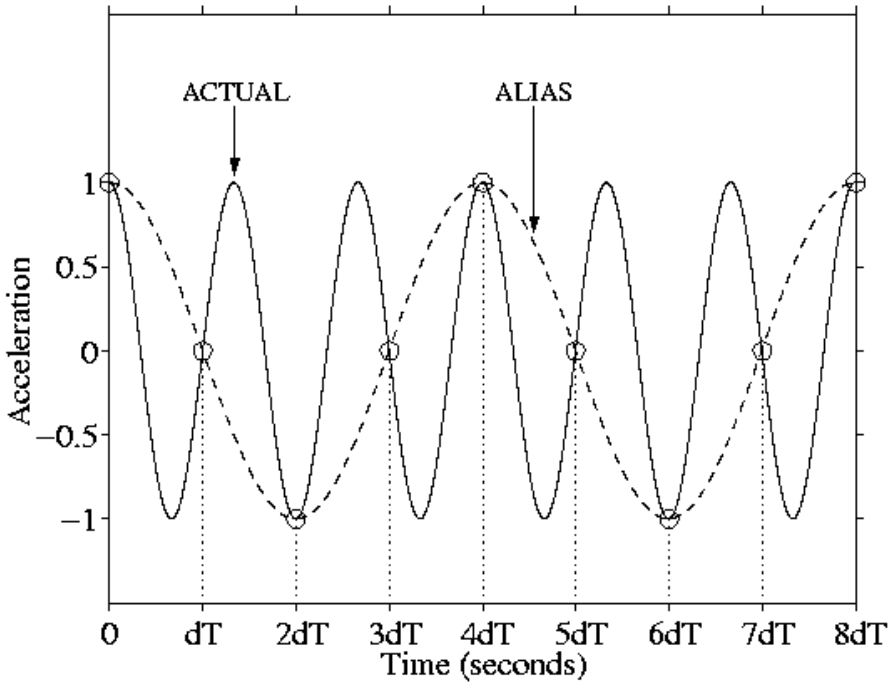

Figure 1. Example of aliasing in time domain. Note that both signals have identical values at sampled points, but the frequencies are different.

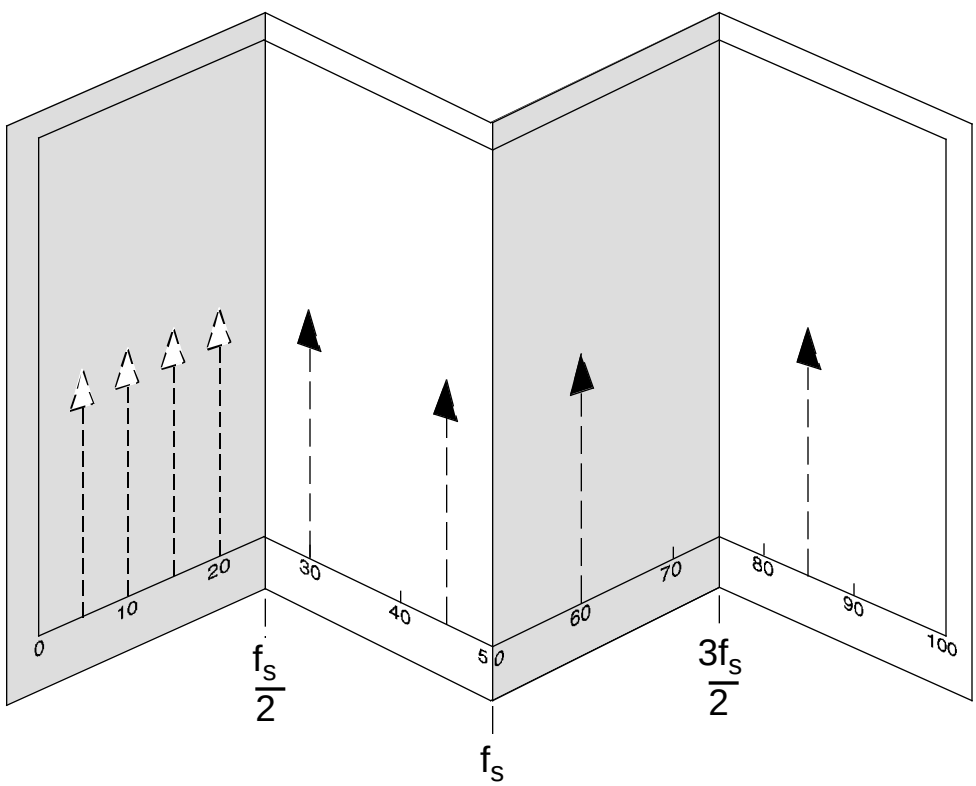

Figure 2. Example of aliasing in frequency domain. Note foldover of spectral components above f_N. For this example, f_S = 50 samples/sec, f_N = 25 Hz.

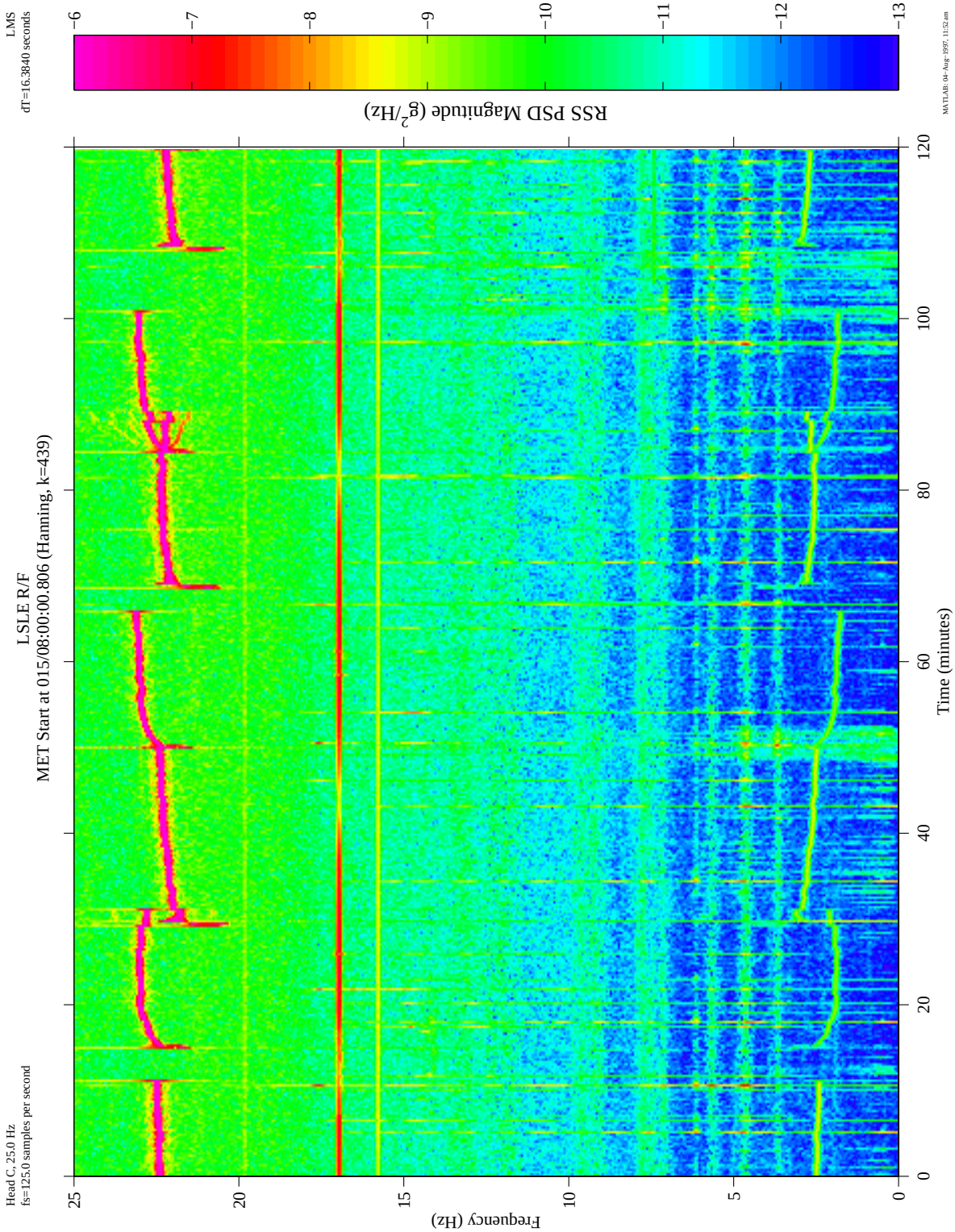

Figure 3. Frequency domain example of aliasing in SAMS data. Upper harmonics of LSLE refrigerator/freezer are folded down to ~2.5 Hz.

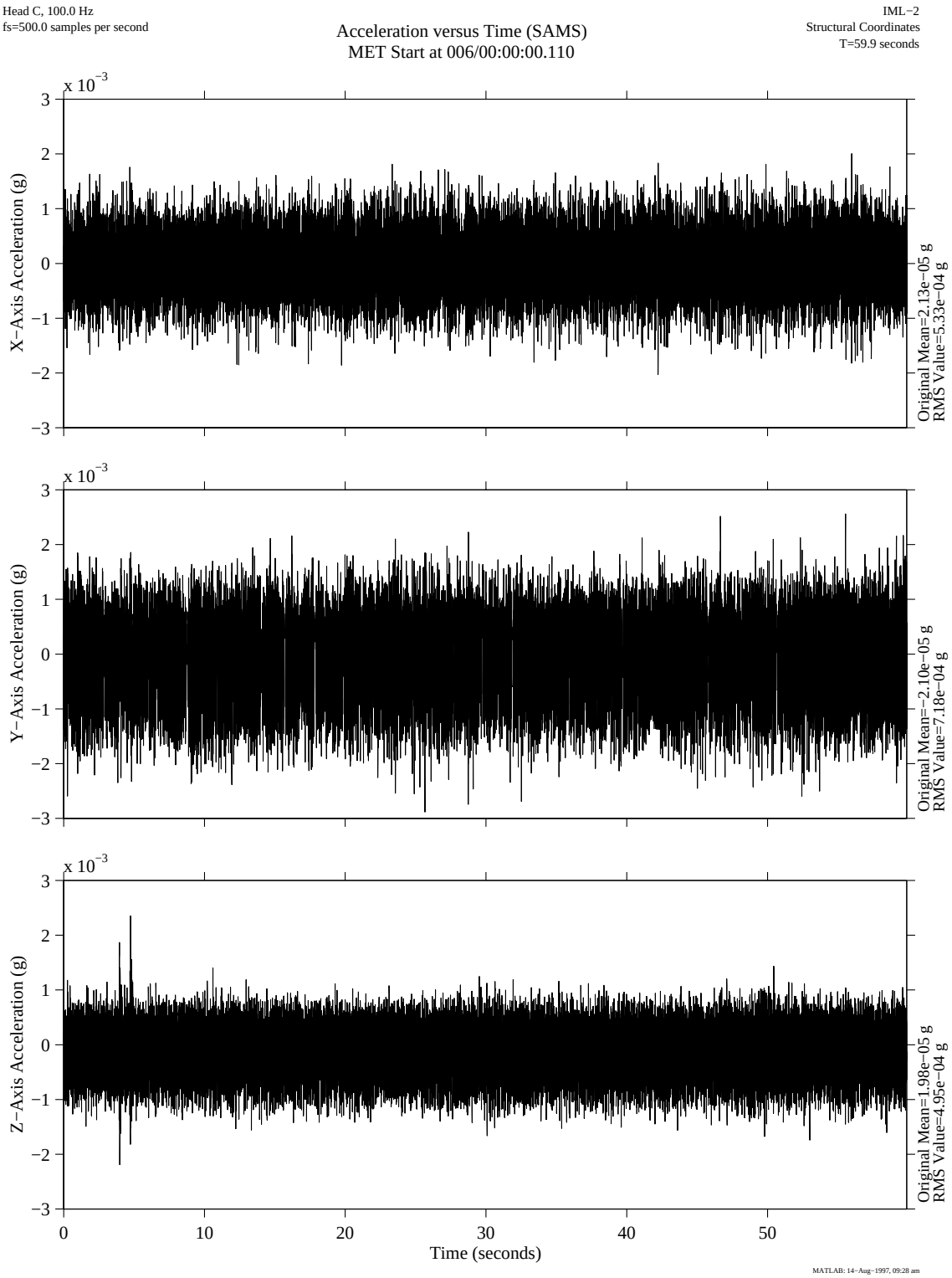

Figure 4. SAMS acceleration versus time plot. One minute's worth of data.

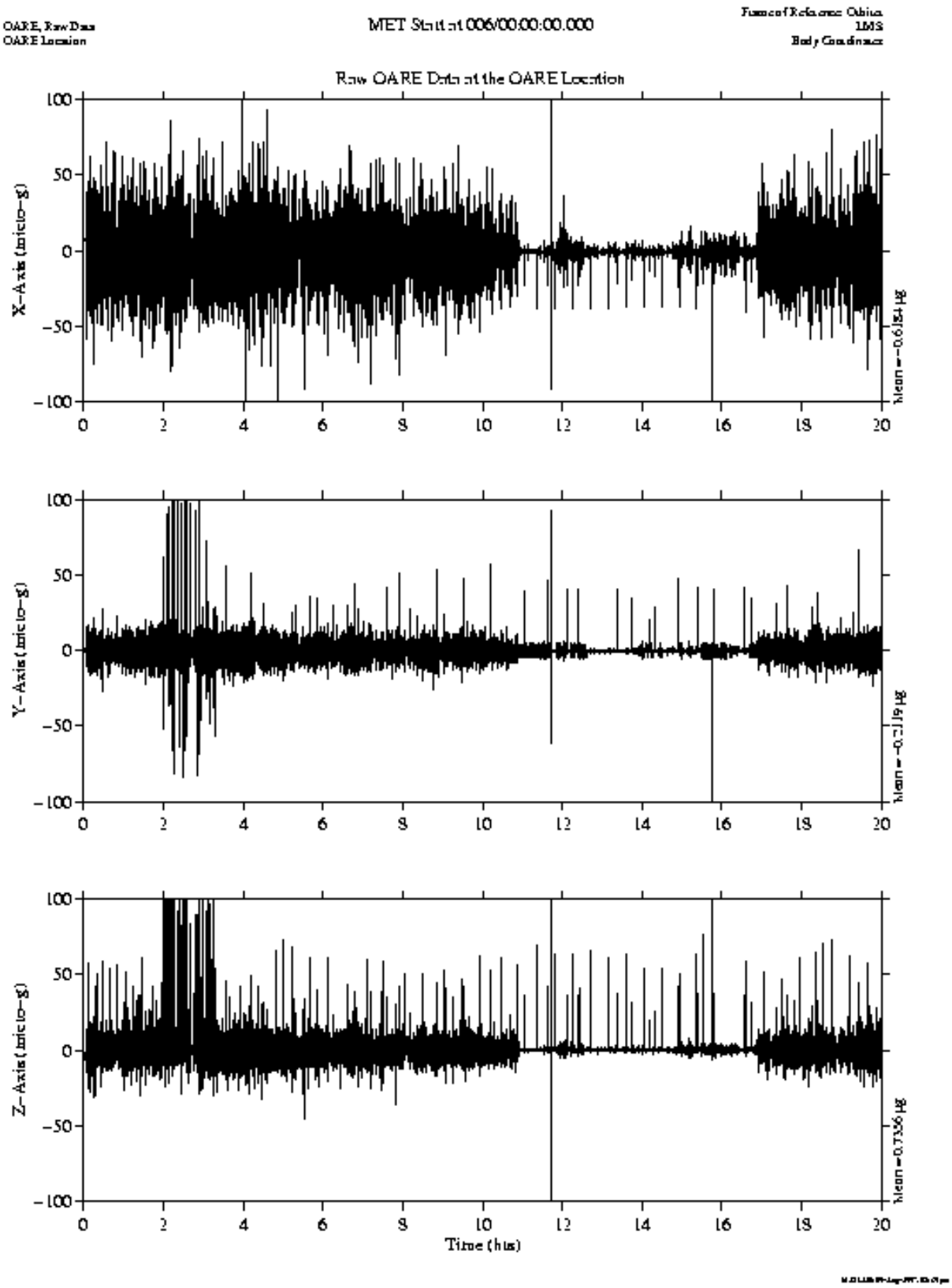

Figure 5. OARE acceleration versus time plot. Twenty hour's worth of data. Note effects of water dump around 2 hours and crew sleep between 11 and 17 hours.

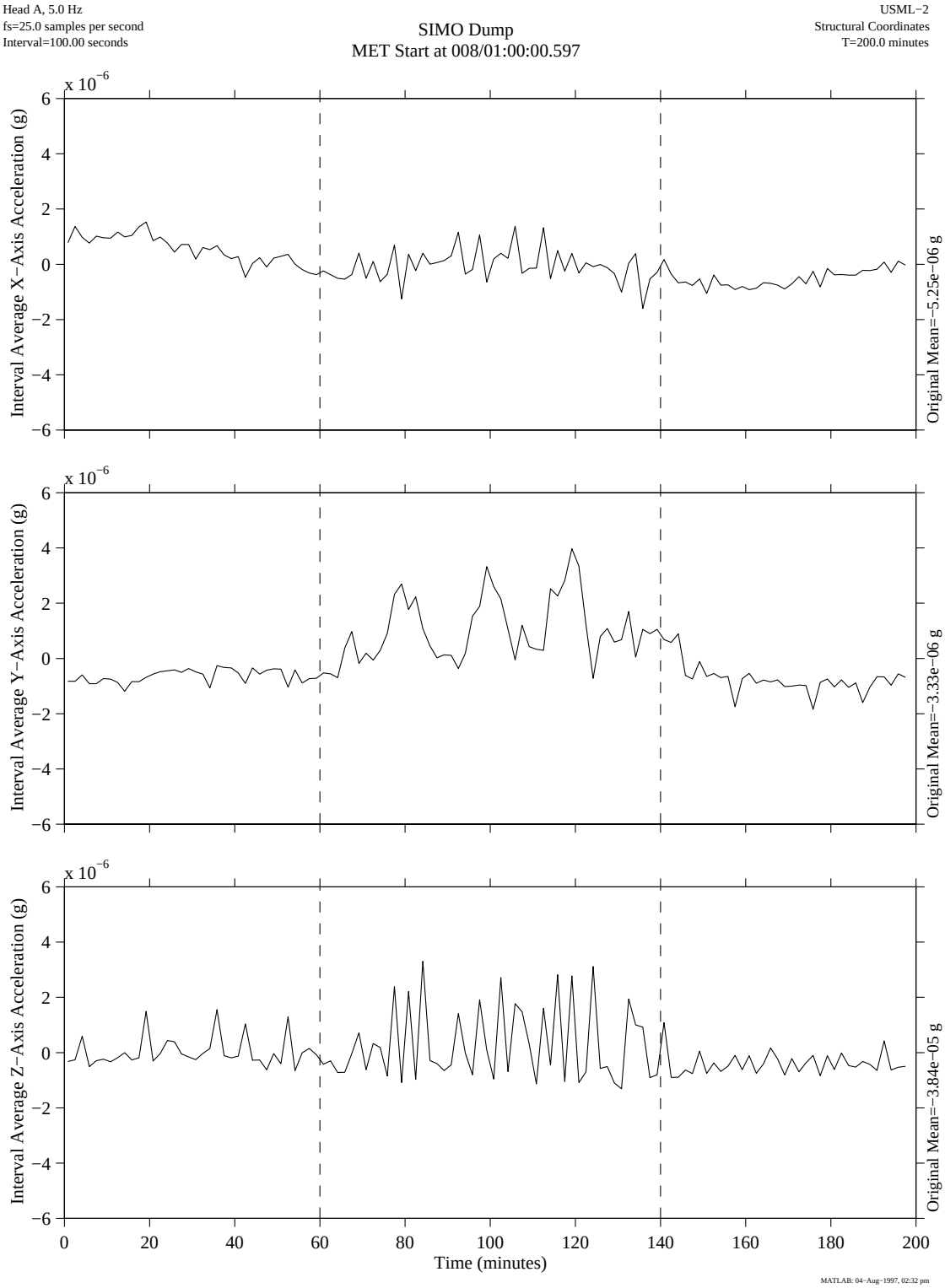

Figure 6. SAMS data with 100 second interval average applied. Two hundred minutes of data plotted. Effects of water dump operations are apparent in center of plots.

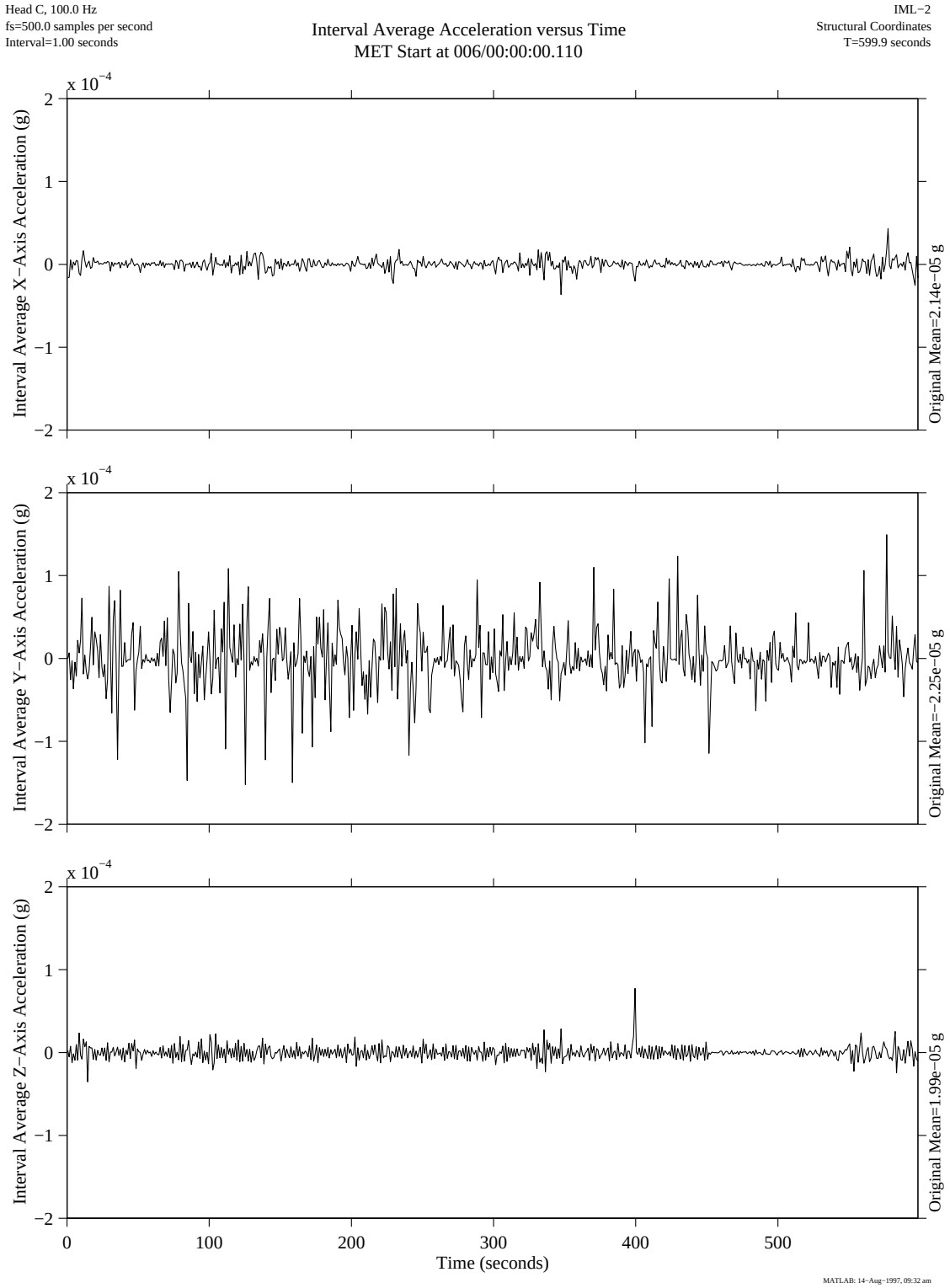

Figure 7. SAMS data with one-second interval average applied. Ten minutes of data plotted. Decrease in levels starting at 450 seconds was caused by cycling off of LSLE refrigerator/freezer compressor.

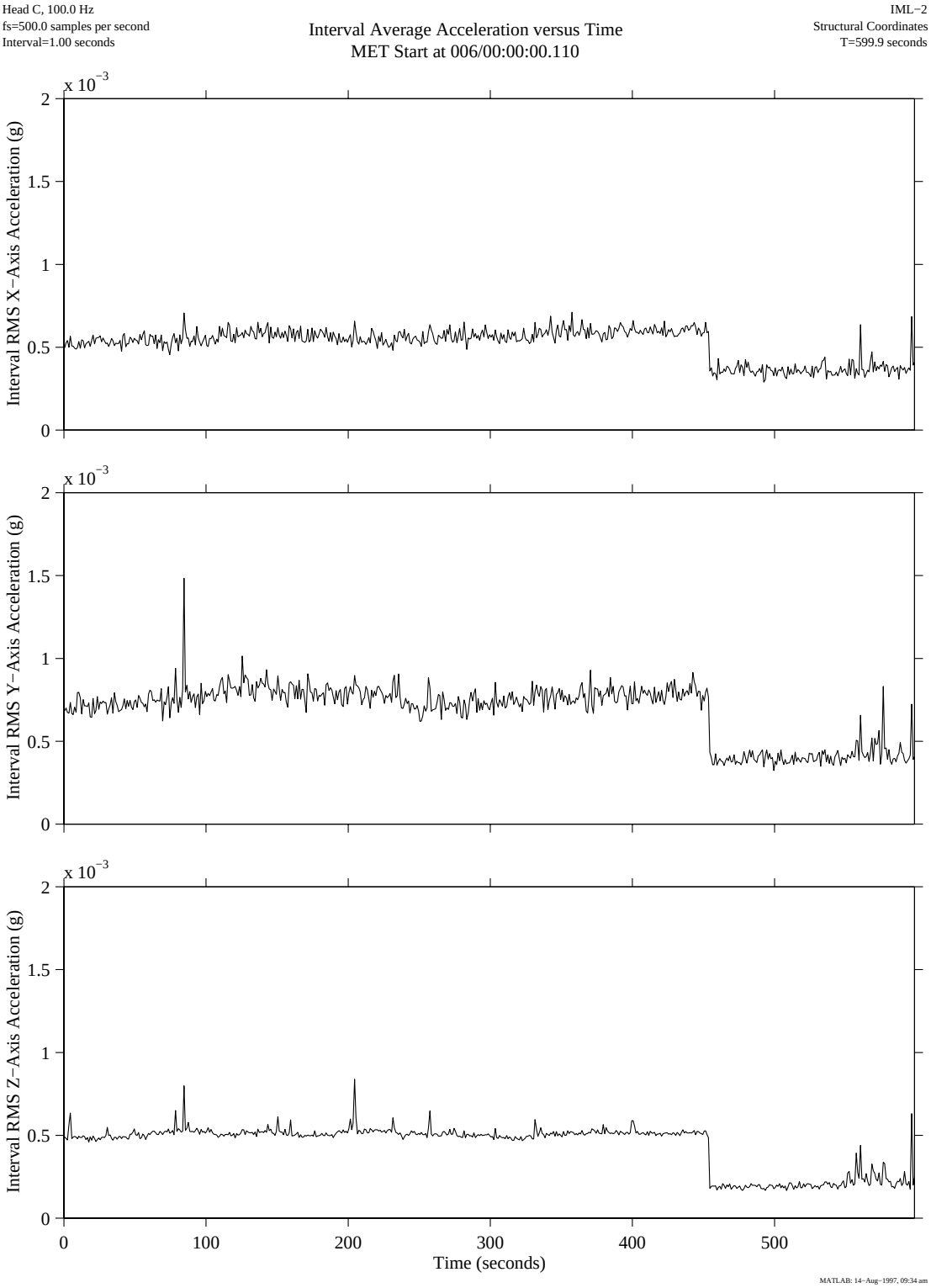

Figure 8. SAMS data with one-second interval RMS applied. Same ten minutes as plotted in Figure 7. Note that the LSLE compressor deactivation is more clearly seen in this plot.

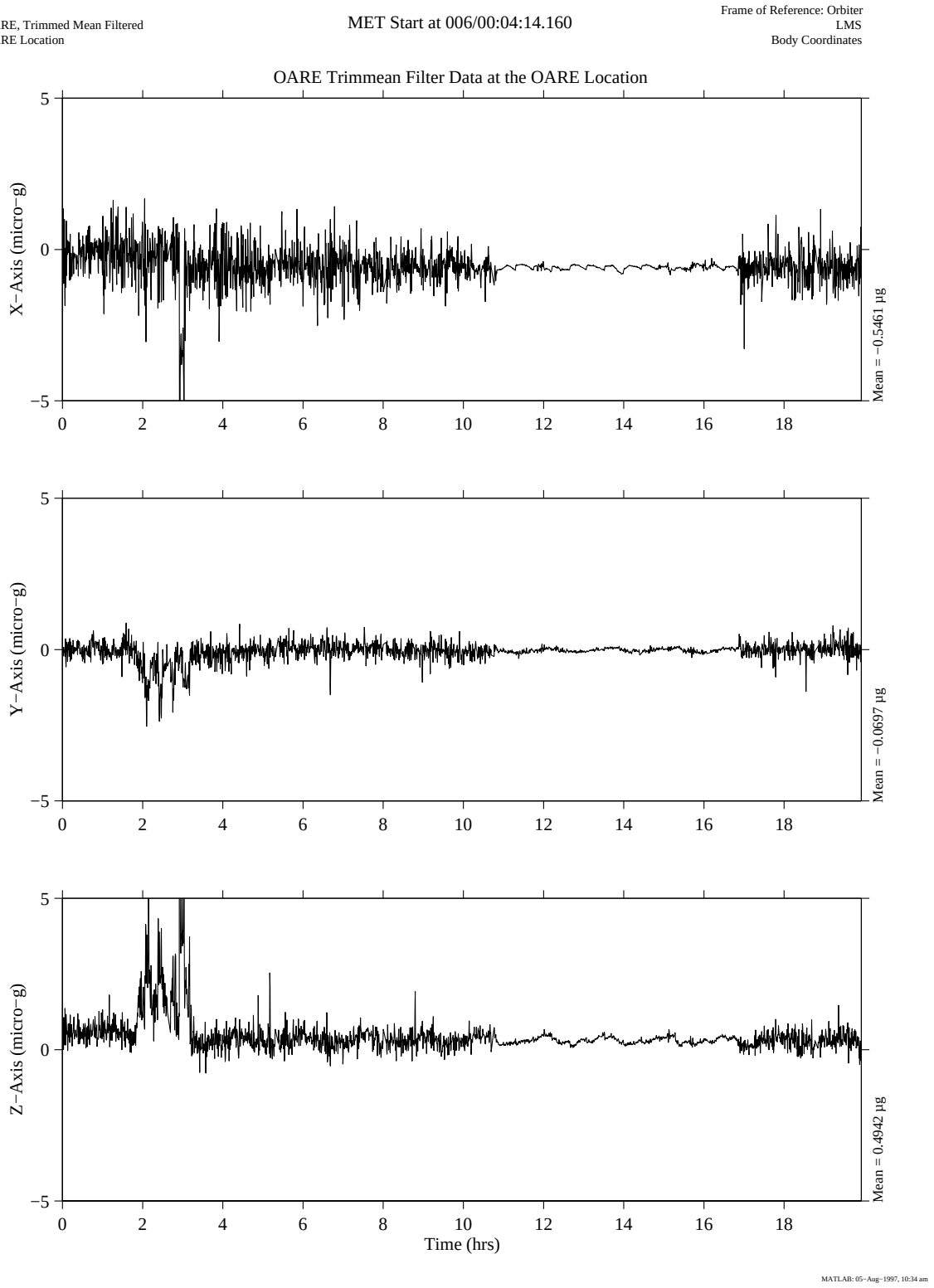

Figure 9. OARE data with trimmean filter applied. Same 20 hours as plotted in Figure 5. Note that transients are reduced and the effects of water dumps, attitude maneuvers, and jet activity during crew sleep are more evident in this plot.

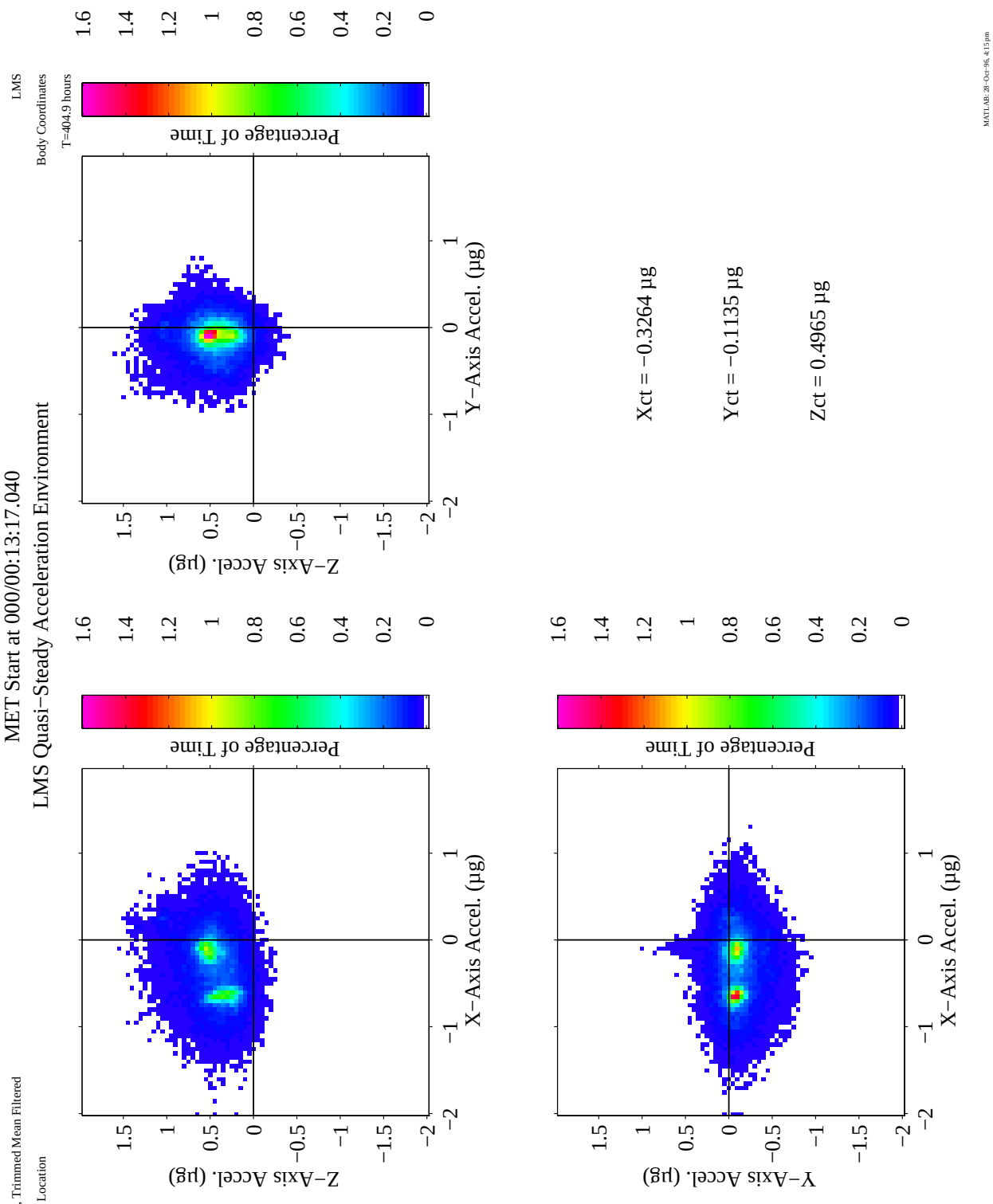

Figure 10. OARE data collected during LMS mission, displayed as quasi-steady three-dimensional histogram. Two clusters of brighter colors in the left-hand display are indicative of the two Orbiter attitudes maintained during the mission.

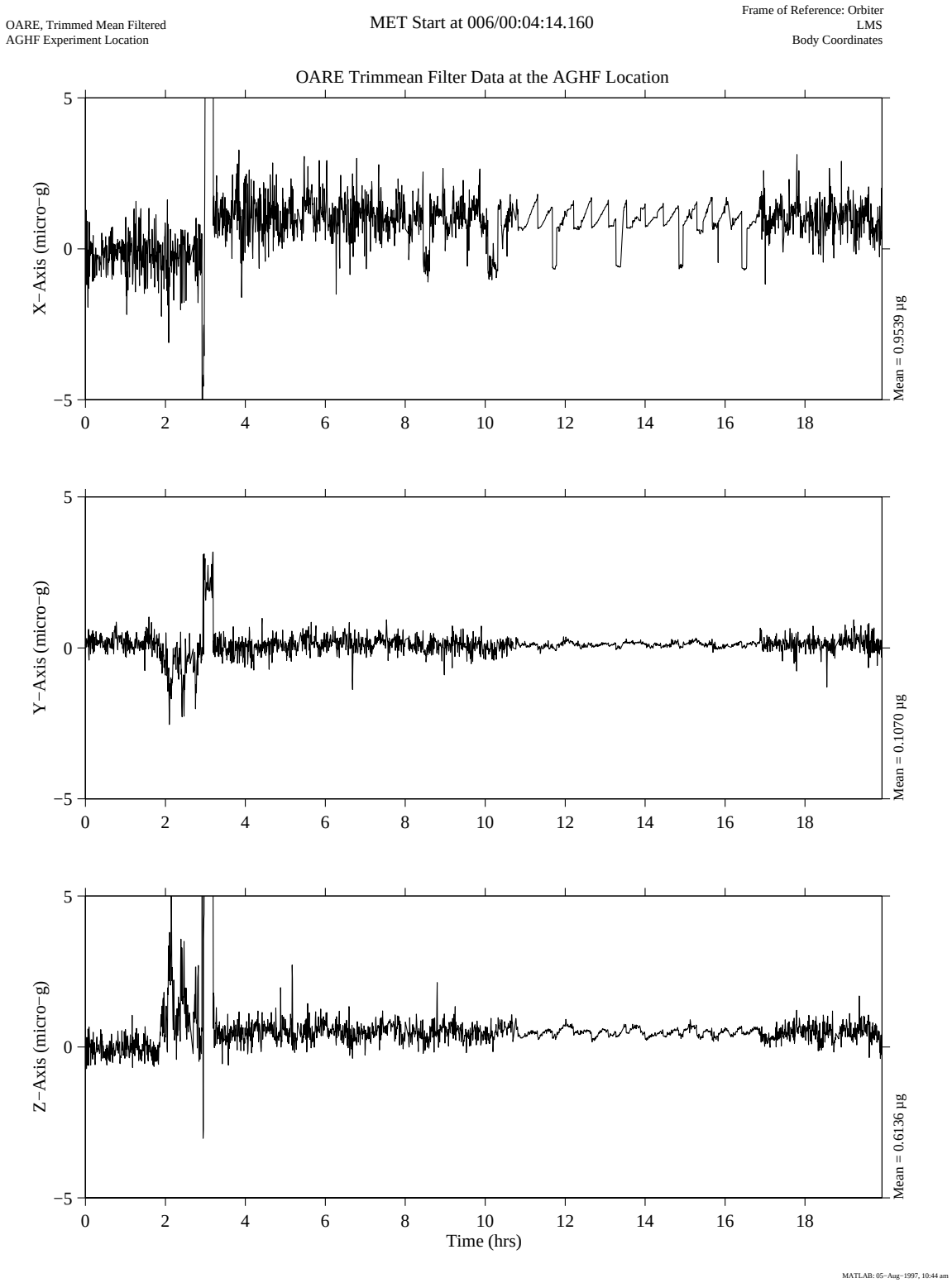

Figure 11. OARE data with trimmean filter applied. Same 20 hours of data plotted in Figure 5, here mapped to the AGHF (Spacelab) location.

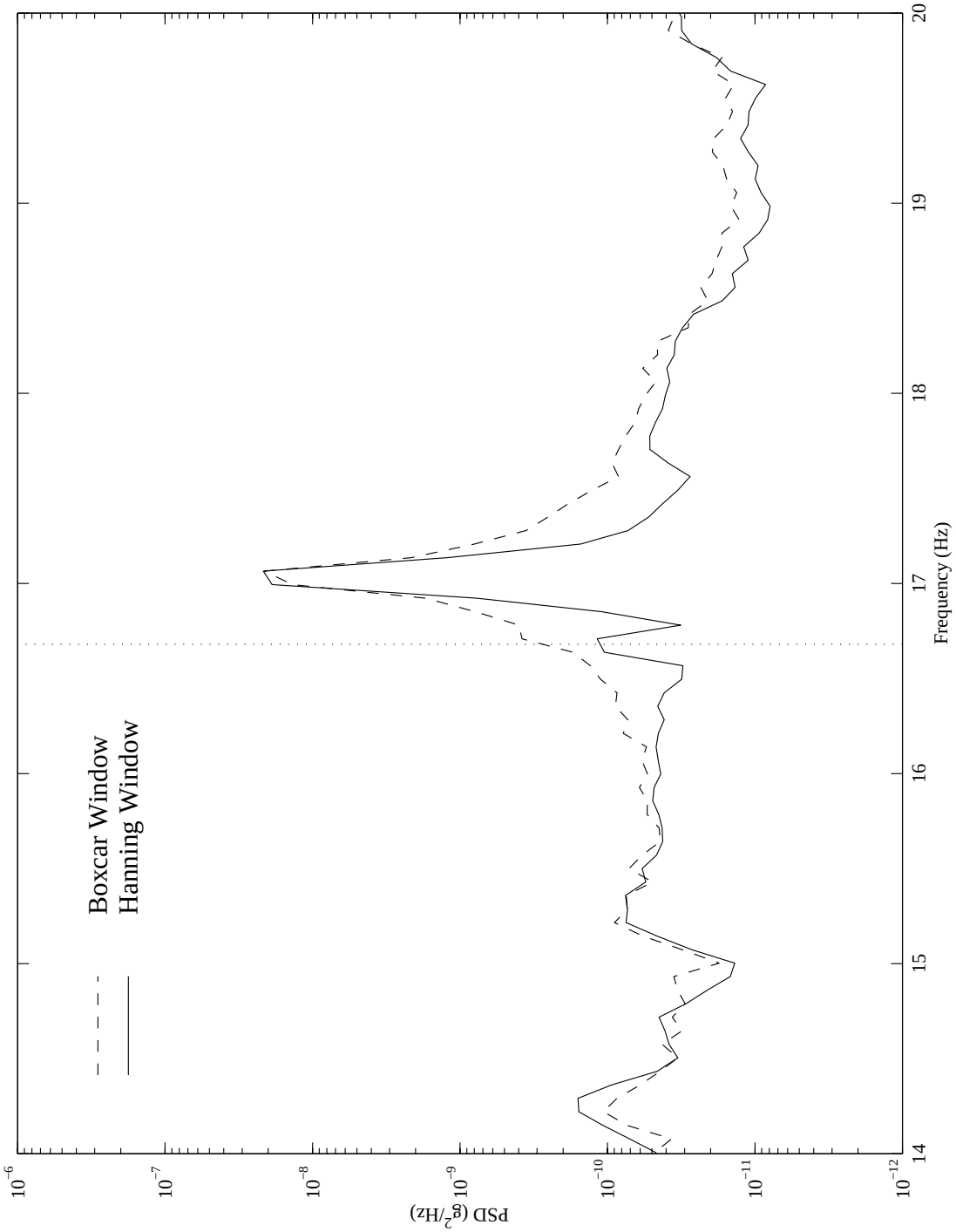

Figure 12. Illustration of spectral leakage obscuring the frequency component at 16.68 Hz.

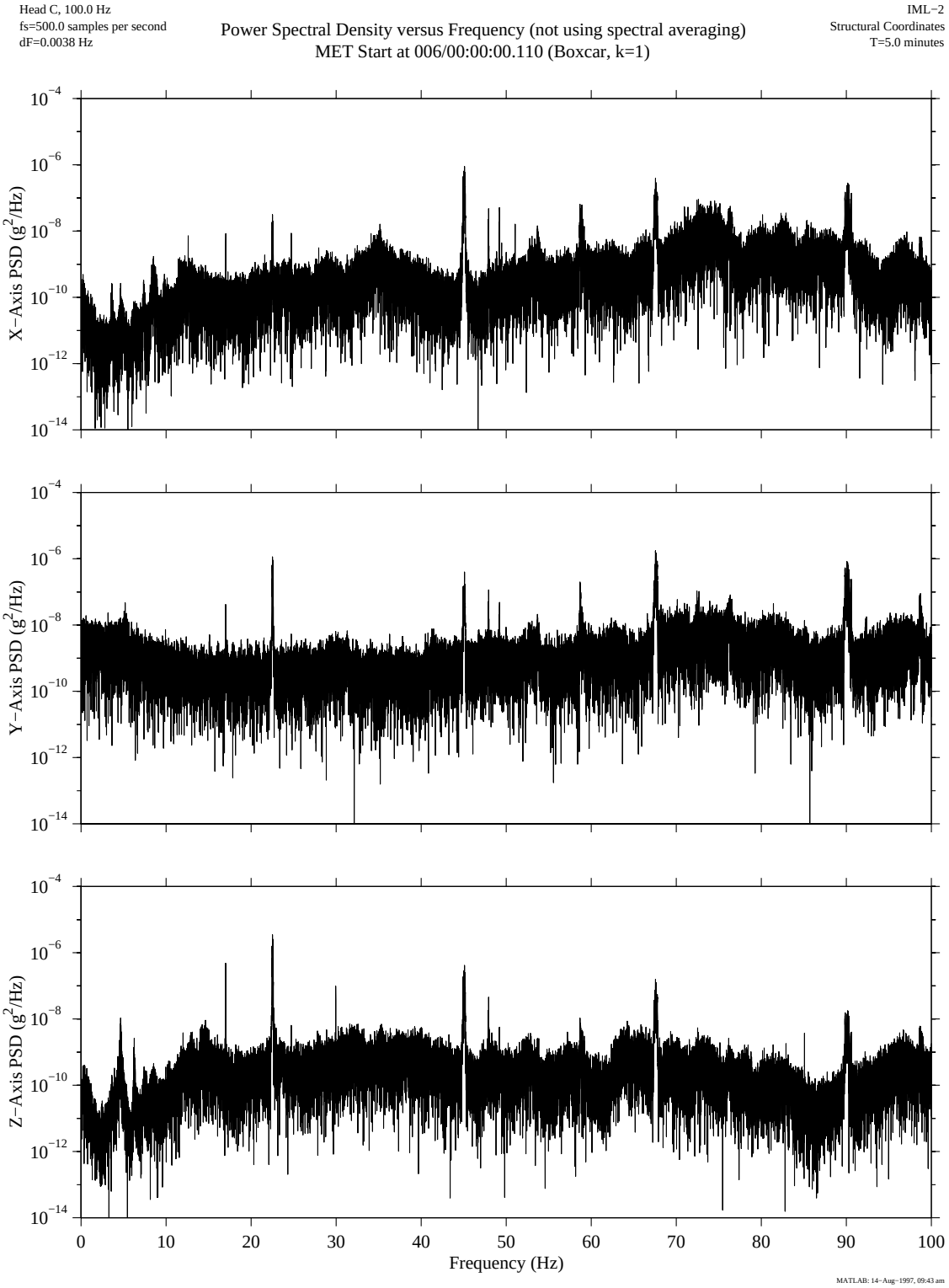

Figure 13. Power spectral density calculated using five minutes of SAMS data. No spectral averaging used.

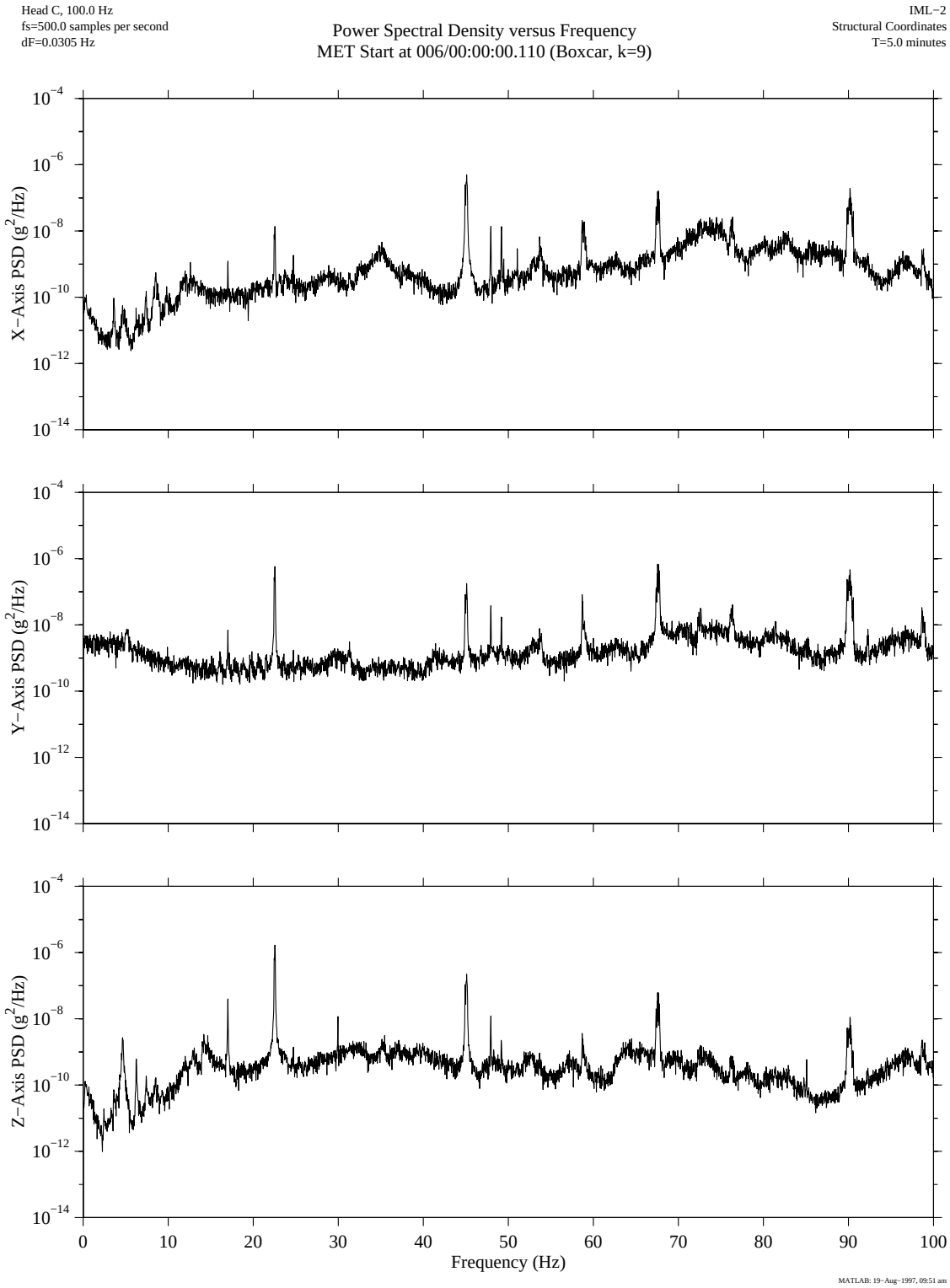

Figure 14. Power spectral density calculated using five minutes of SAMS data. The data were divided into nine consecutive segments and the PSDs for the nine segments were averaged together point by point. Compare to Figure 13 which was not averaged.

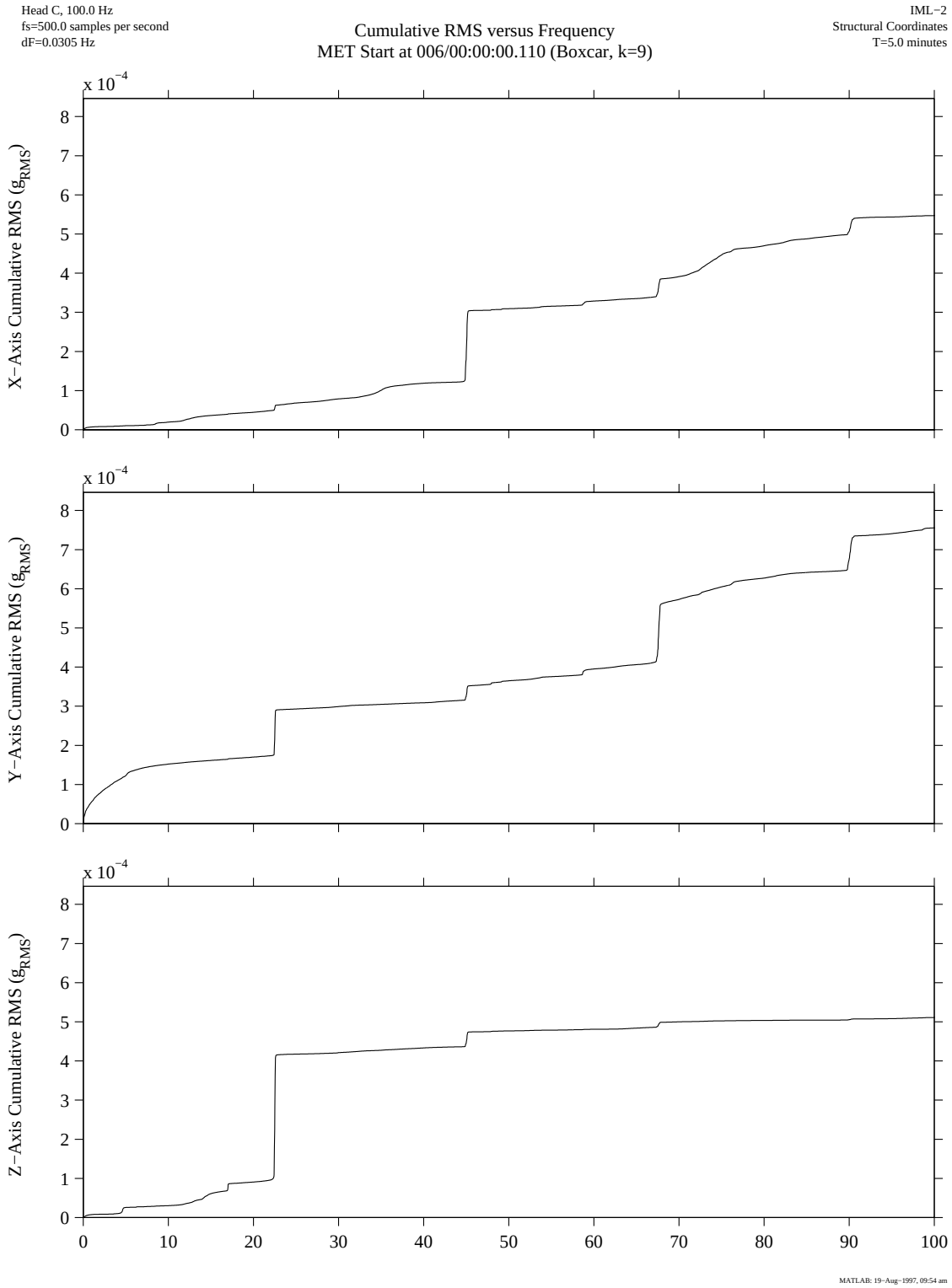

Figure 15. SAMS data displayed as cumulative RMS acceleration versus frequency. Same time period as displayed in Figure 14. Note steps appear in plots at excited frequencies.

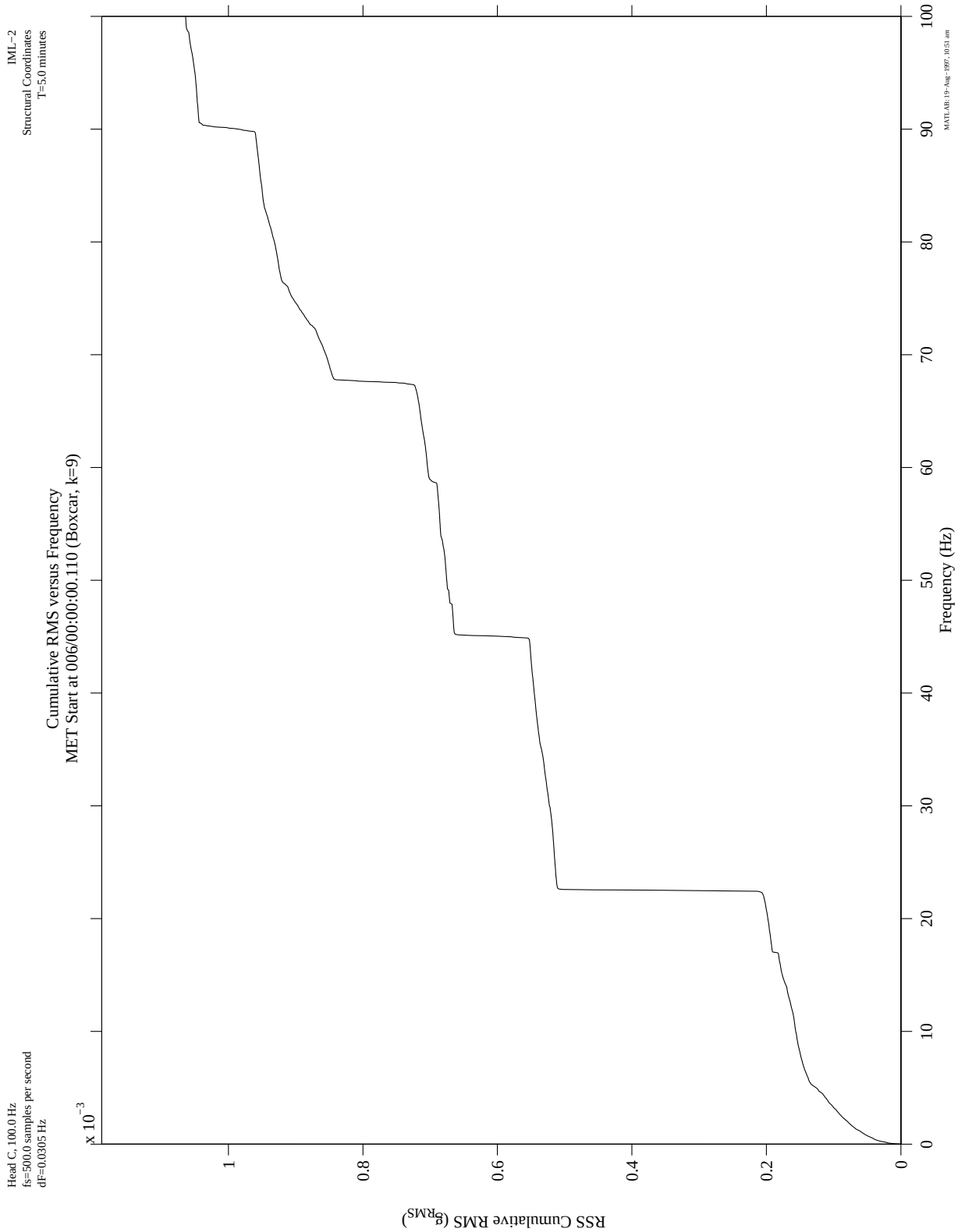

Figure 16. RSS of individual axes of SAMS data displayed as cumulative RMS acceleration versus frequency. Same period as previous figure.

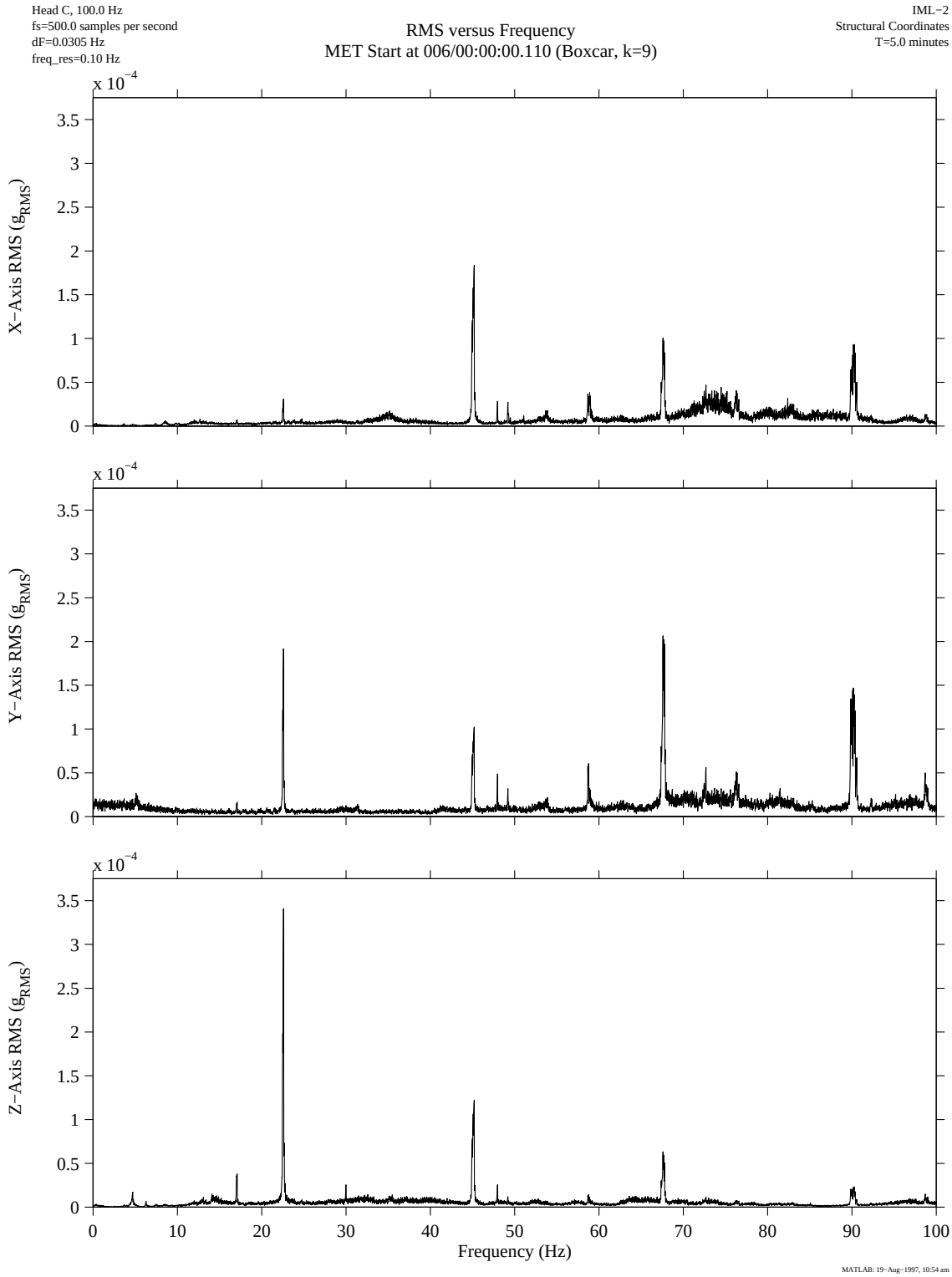

Figure 17. SAMS data displayed as g_{RMS} versus frequency. RMS levels computed for 0.1 Hz wide bands. Same time period as figures 14-16.

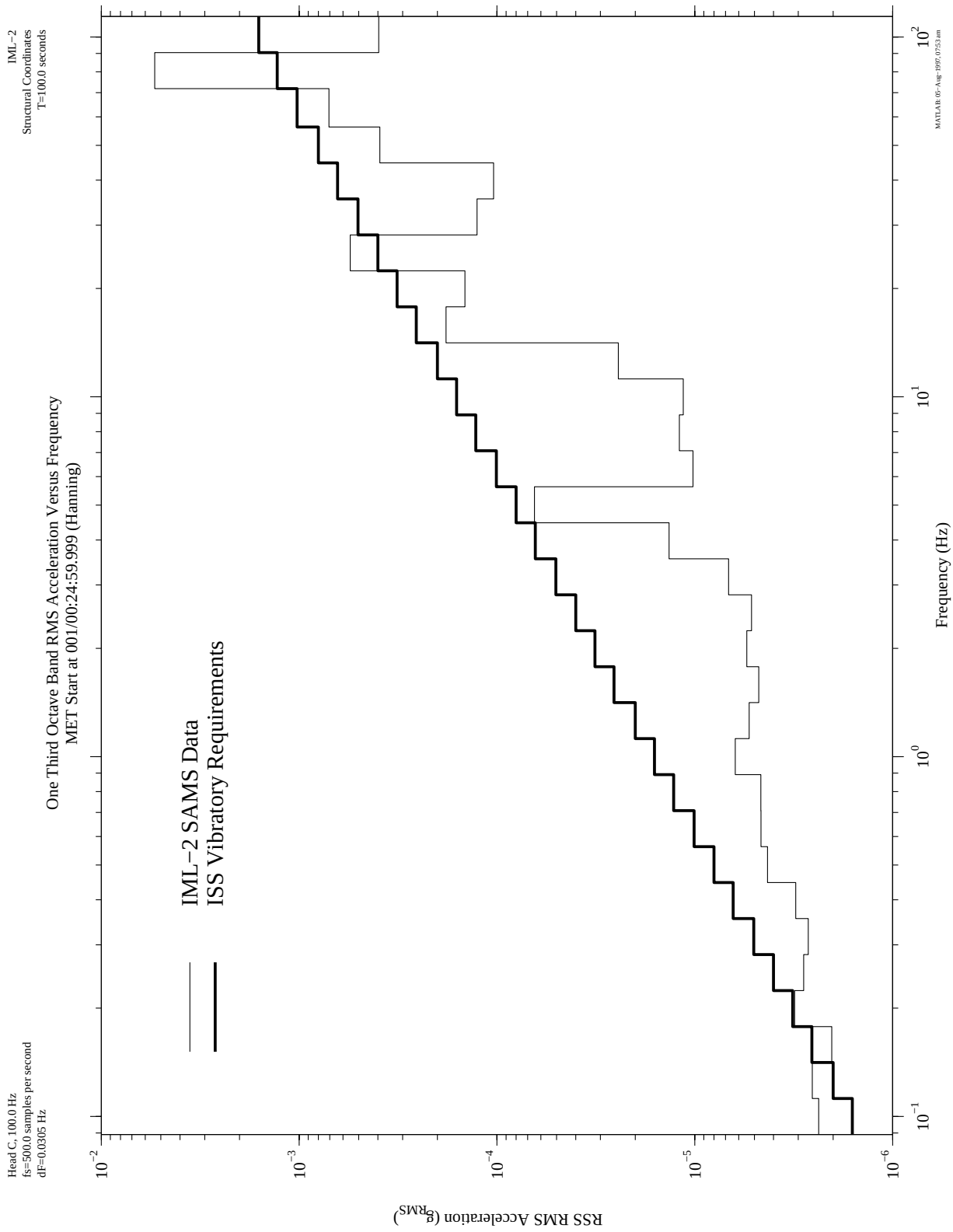

Figure 18. RSS one third octave RMS acceleration versus frequency using 100 seconds of SAMS data. Bold line is current ISS vibratory requirements curve.

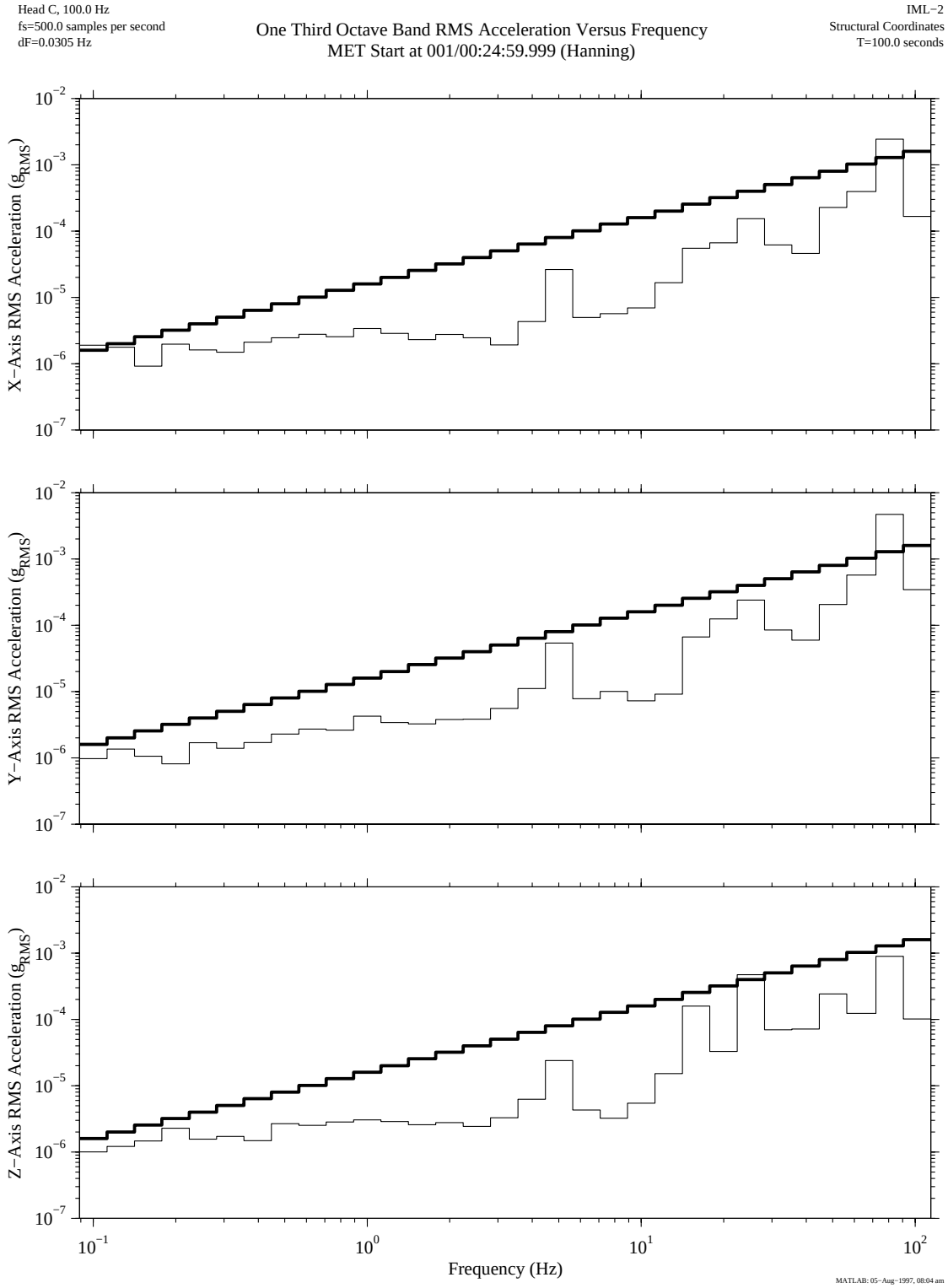

Figure 19. Three axes of SAMS data plotted as one third octave RMS acceleration versus frequency. Same time period as Figure 18.

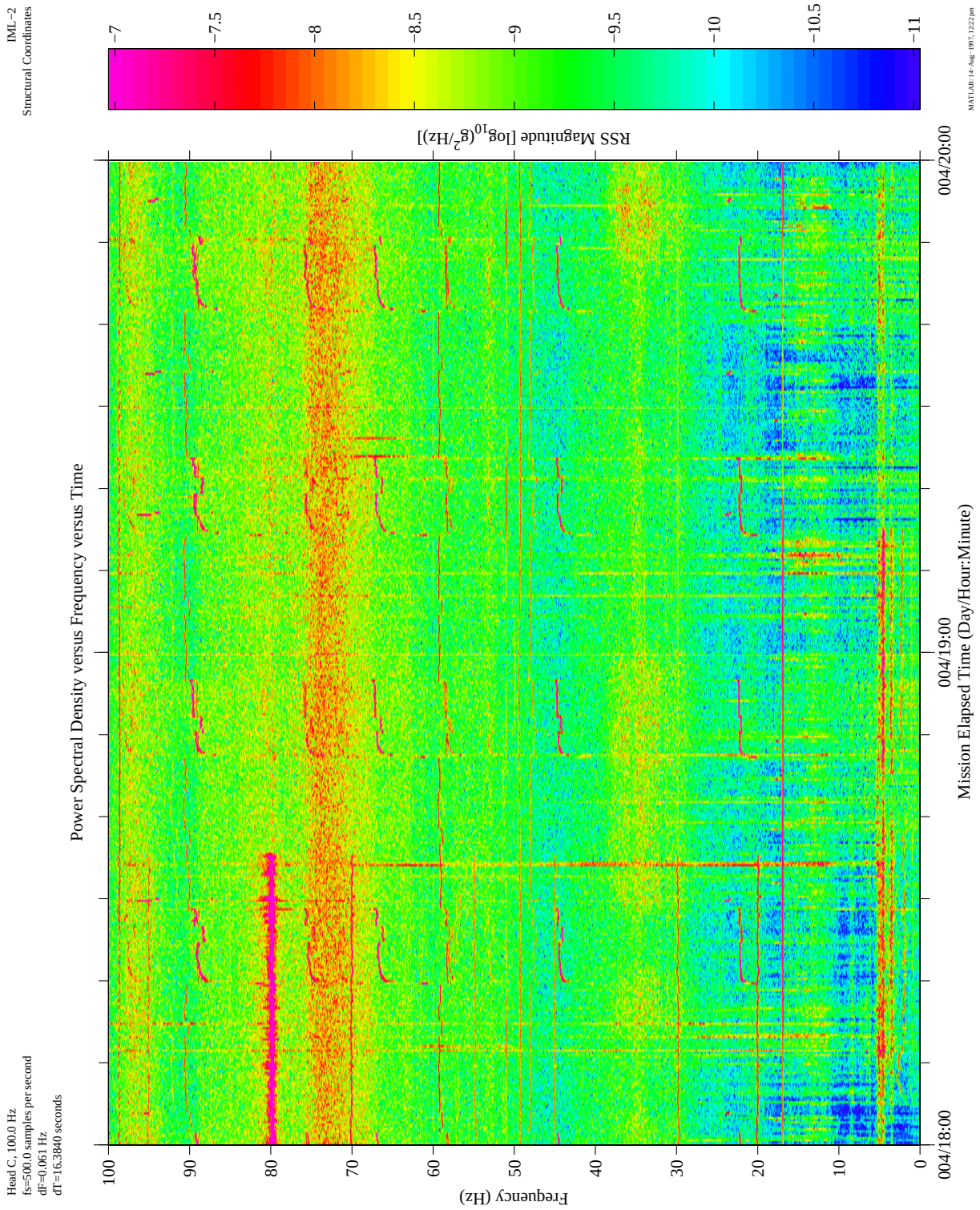

Figure 20. Power spectral density versus frequency versus time for two hours of SAMS data. Three axes PSDs were combined using RSS prior to creation of spectrogram. Note cessation of 80 Hz TEMPUS pump 33 minutes into plot and regular cycling of LSLE compressor about 22 Hz (and upper harmonics).

$$\underbrace{a}_{❶}\underbrace{x}_{❷}\underbrace{m}_{❸}\underbrace{00}_{❹}\underbrace{10}_{❹}\underbrace{2}_{❺}.\underbrace{1}_{❻}\underbrace{5}_{❼}\underbrace{r}_{❽}$$

1) Sensor Head (a,b,c)

2) Axis (x,y,z)

3) Time Reference : $\begin{cases} \text{m : Mission Elapsed Time} \\ \text{n : Near Mission Elapsed Time} \\ \text{r : Russian Time} \\ \text{g : Greenwich Mean Time} \end{cases}$

4) Day: 3 digits, with leading zeros

5) Hour: 2 digits, with leading zeros

6) File Number (1,2,3,4,5,6)

7) Total number of files per hour (1,2,4,5,6)

8) Type of data in file : $\begin{cases} \text{r : Reduced acceleration data} \\ \text{g : Gain setting information} \\ \text{t : Temperature data} \end{cases}$

Figure 21. SAMS data naming convention.

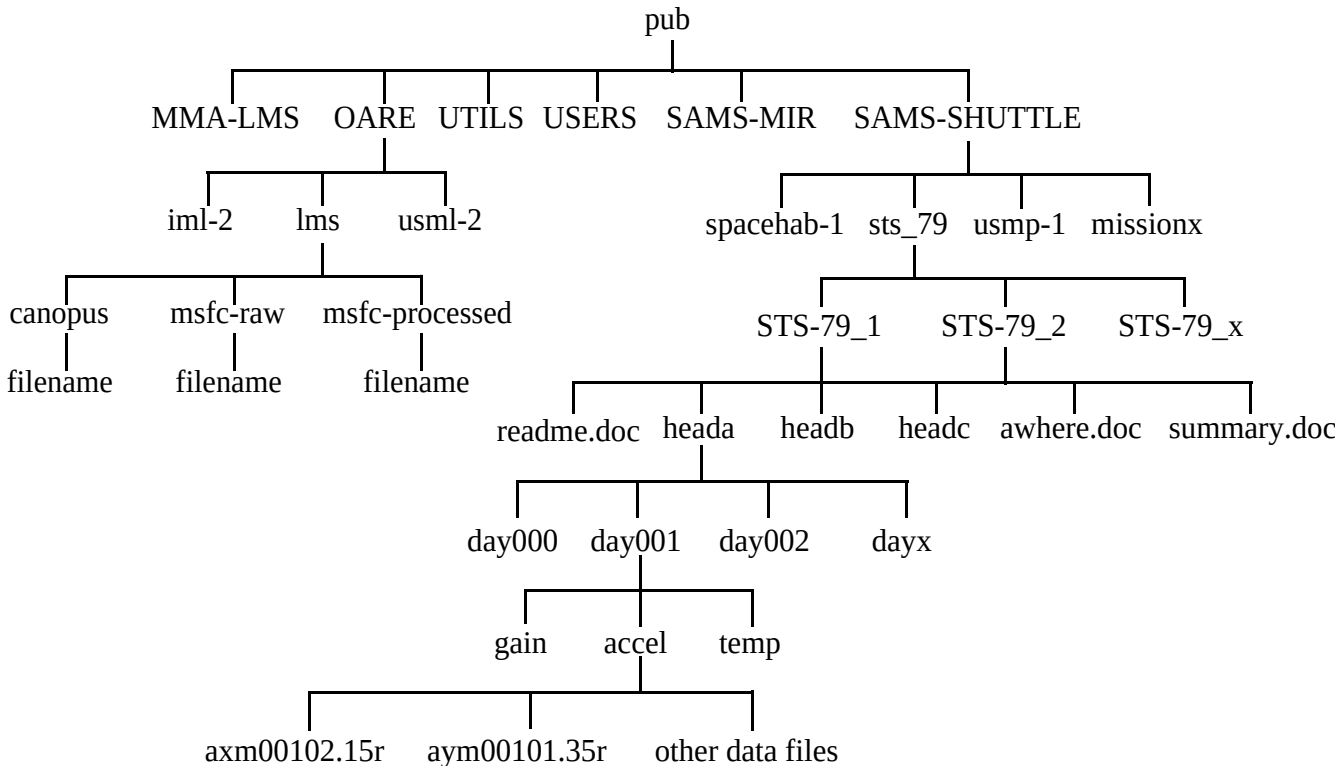

Figure 22. Accessing Acceleration Data via the Internet from beech.lerc.nasa.gov